HHS Public Access

Author manuscript

Cell Rep. Author manuscript; available in PMC 2024 September 30.

Published in final edited form as:

Cell Rep. 2024 August 27; 43(8): 114565. doi:10.1016/j.celrep.2024.114565.

MicroRNA-19b exacerbates systemic sclerosis through promoting Th9 cells

Yun-Ji Lim[1], **Sang-A Park**[1,5], **Dandan Wang**[2], **Wenwen Jin**[1], **Wai Lim Ku**[3], **Dunfang Zhang**[1], **Junji Xu**[1], **Liliana C. Patiño**[1], **Na Liu**[1], **Weiwei Chen**[2], **Rida Kazmi**[1], **Keji Zhao**[3], **Ying E. Zhang**[4], **Lingyun Sun**[2,*], **WanJun Chen**[1,6,*]

[1]Mucosal Immunology Section, National Institute of Dental and Craniofacial Research, National Institutes of Health, 30 Convent Drive, Bethesda, MD 20892, USA

[2]Department of Rheumatology and Immunology, Nanjing Drum Tower Hospital, Affiliated Hospital of Medical School, Nanjing University, Nanjing 210008, China

[3]Systemic Biology Center, National Heart, Lung, and Blood Institute, National Institutes of Health, 31 Center Drive, Bethesda, MD 20892, USA

[4]Laboratory of Cellular and Molecular Biology, Center for Cancer Research, National Cancer Institute, National Institutes of Health, 37 Convent Drive, Bethesda, MD 20892, USA

[5]Deceased

[6]Lead contact

SUMMARY

Systemic sclerosis (SSc) is a chronic autoimmune disease characterized by fibrosis of the skin and multiple vital organs, but the immunological pathogenesis of SSc remains unclear. We show here that *miR-19b* promotes Th9 cells that exacerbate SSc. Specifically, *miR-19b* and interleukin (IL)-9 increase in $CD4^+$ T cells in experimental SSc in mice induced with bleomycin. Inhibiting *miR-19b* reduces Th9 cells and ameliorates the disease. Mechanistically, transforming growth factor beta (TGF-β) plus IL-4 activates pSmad3-Ser^{213} and TRAF6-K63 ubiquitination by suppressing NLRC3. Activated TRAF6 sequentially promotes TGF-β-activated kinase 1 (TAK1) and nuclear factor κB (NF-κB) p65 phosphorylation, leading to the upregulation of *miR-19b*. Notably, *miR-19b* activated *Il9* gene expression by directly suppressing atypical E2F family member E2f8. In patients with SSc, higher levels of *IL9* and *MIR-19B* correlate with worse

*Correspondence: lingyunsun@nju.edu.cn (L.S.), wchen@nih.gov (W.C.).

AUTHOR CONTRIBUTIONS

Y.-J.L. and S.-A.P designed the experiments and Y.-J.L. performed most of the experiments, analyzed data, and drafted the manuscript. D.W. and Weiwei Chen designed and performed clinical studies in patients with SSc and drafted the manuscript. W.J., W.L.K., D.Z., J.X., L.C.P., and N.L. performed experiments and/or collected and analyzed data. R.K. performed mouse administration and PCR genotyping. K.Z. and Y.E.Z. provided crucial scientific input and/or research materials, supervised experiments, and edited the manuscript. L.S. supervised and designed clinical studies with patients with SSc. WanJun Chen conceived and supervised the whole research, designed the experiments, and wrote the manuscript.

DECLARATION OF INTERESTS

The authors declare no competing interests.

SUPPLEMENTAL INFORMATION

Supplemental information can be found online at https://doi.org/10.1016/j.celrep.2024.114565.

disease progression. Our findings reveal *miR-19b* as a key factor in Th9 cell-mediated SSc pathogenesis and should have clinical implications for patients with SSc.

In brief

Lim et al. find that TGF-β and IL-4 induce *miR-19b* via the TRAF6-TAK1-NF-κB axis, upregulating IL-9 in $CD4^+$ T cells. Blockade of IL-9 and *miR-19b* in a SSc mouse model suppresses fibrogenesis. Importantly, increased *IL9* and *MIR-19B* in patients with SSc correlates with scleroderma pathogenesis.

Graphical Abstract

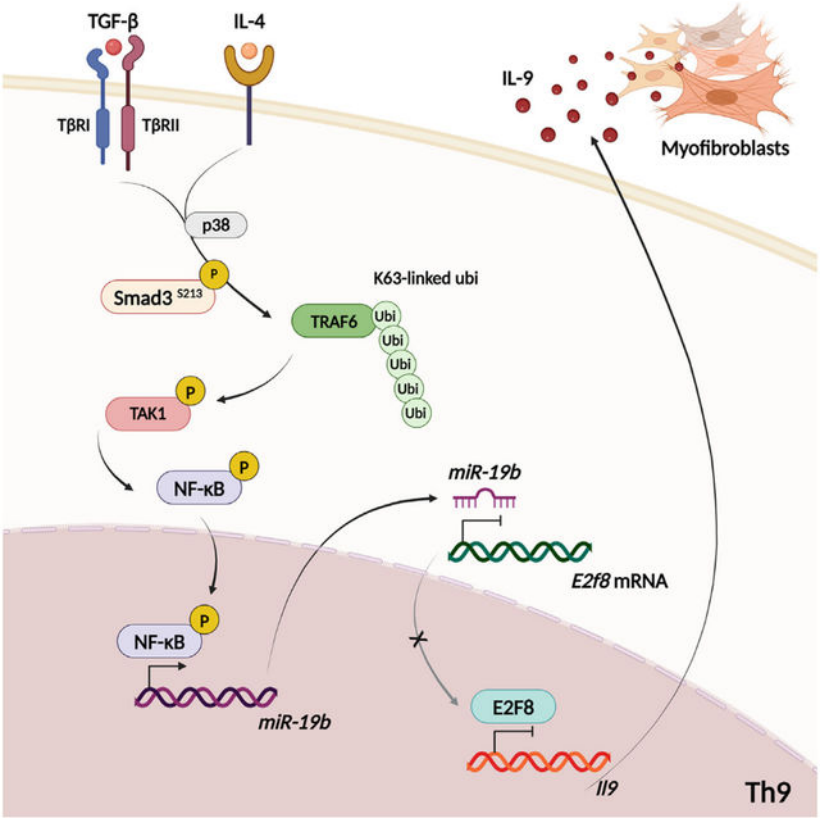

INTRODUCTION

Systemic sclerosis (SSc) is a chronic autoimmune disease in which abnormal immune responses lead to the activation and expansion of autoreactive effector immune cells, resulting in fibrosis of the skin and multiple internal organs.[1] Recently, it has been reported that interleukin (IL)-4 and transforming growth factor beta (TGF-β) are increased in the serum and affected tissues of patients with SSc,[2] but the impact and mechanisms of the elevation of these cytokines remain unknown.

IL-4 and TGF-β signaling induces the differentiation of Th9 cells in both murine and human naive $CD4^+$ T cells.[3–5] TRAF6 is considered as a key mediator for transducing noncanonical

signaling downstream of TGF-β by direct interaction with TGF-β receptors (TβRs)[6,7] and has been reported to play a role for Th9 cell proliferation through the nuclear factor κB (NF-κB) pathway in response to certain costimulatory stimuli including OX40 (tumor necrosis factor receptor superfamily 4, *Tnfrs4*) and glucocorticoid-induced tumor necrosis factor receptor during Th9 differentiation.[8] However, whether TRAF6 is directly involved in Th9 differentiation in response to IL-4 plus TGF-β stimulation remains unknown.

Smad3 has been reported to be important in Th9 differentiation.[9,10] We recently reported that the phosphorylation of Smad3 at linker Ser^{213} and the ensuing upregulation of albumin D-box binding protein (DBP) and downregulation of E2f8 are the key regulators for *Il9* gene transcription.[5] However, it is not yet clear whether and how the TRAF6-mediated pathway and Smad3-mediated signaling interact with and regulate each other during Th9 differentiation in response to IL-4 and TGF-β.

MicroRNAs (miRNAs) are small noncoding RNAs that play critical roles in regulating the expression of target genes.[11] Most miRNAs are transcribed from DNA sequences into primary miRNAs and processed into precursor miRNAs and then mature miRNAs (~19–24 nt long).[11] miRNAs interact with the 3′ untranslated region (UTR) of target mRNAs to induce mRNA degradation and translation repression.[12] Many studies have suggested that miRNAs are involved in regulating the secretion of inflammatory cytokines and the proliferation, differentiation, and functional maintenance of T cells.[11,13–15] For example, *miR-19b* is known as a major oncogenic miRNA of the *miR-17–92* cluster and promotes the differentiation of Th1,[16] Th2,[17] and Th17 cells[18] while limiting inducible regulatory T (Treg) cell differentiation.[16] However, the role of *miR-19b* in Th9 cells remains unclear.

In this study, we have uncovered that IL-4 and TGF-β signaling induces TRAF6 K63 ubiquitination (Ub) through phosphorylated Smad3-Ser^{213}. TRAF6 activation consequently forms a complex with and activates TGF-β-activated kinase 1 (TAK1), which increases NF-κB p65 phosphorylation leading to the expression of *miR-19b*. The expression of *miR-19b* promotes *Il9* gene expression by targeted *E2f8* gene suppression during Th9 differentiation. Notably, *miR-19b* is elevated in $CD4^+$ T cells in experimental SSc in mice and from patients with SSc and plays a key role in the pathogenesis of SSc by enhancing Th9 cells. Our findings are expected to have implications for targeting *miR-19b* and Th9 cells in developing potential therapy for human SSc.

RESULTS

TGF-β and IL-4 signaling induces TRAF6 in T cells

TRAF6 is a key mediator for transducing signaling downstream of TGF-β signaling to activate TAK1[5,7,19]; however, it is unknown whether IL-4 and TGF-β signaling directly controls the expression and function of TRAF6. We firstly studied *Traf6* gene expression in normal naive $CD4^+$ T cells stimulated with T cell receptors (TCRs; anti-CD3 and anti-CD28) in the presence of TGF-β, IL-4, or a combination of the two in cultures. At the mRNA level, we found that the addition of IL-4 stimulation for 2 h induced a significant increase in the *Traf6* gene compared to TCR stimulation alone; the addition of TGF-β alone at the same time, however, failed to do so (Figure 1A). Consequently, IL-4 plus TGF-β

increased similar amounts of *Traf6* to IL-4 stimulation alone (Figure 1A). In contrast to IL-4, other Th2 cytokines such as IL-5 and IL-13 were unable to induce any increase in *Traf6* mRNA in TCR-stimulated T cells (Figure S1A), suggesting a significant feature for IL-4 in early *Traf6* induction. Unexpectedly, this IL-4-mediated early increase in *Traf6* mRNA was completely abolished in naive $CD4^+$ T cells with the deletion of TβRI (*Tgfbr1* knockout [KO], *Tgfbr1*$^{f/f}$-ER^{Cre} mice treated with tamoxifen for 5 days) (Figures 1A and S1A). In contrast to *Traf6* mRNA expression that was sufficiently induced by IL-4 alone, however, analysis of TRAF6 protein with western blots revealed that it was increased only by IL-4 plus TGF-β stimulation but not either one alone (Figure 1B). Similar to mRNA, the increased TRAF6 protein by IL-4 plus TGF-β was also completely abrogated in the *Tgfbr1* KO $CD4^+$ T cells (Figure 1B). Kinetic studies showed that the increase in TRAF6 protein by IL-4 plus TGF-β also peaked at 2 h but subsided by 4 h following stimulation (Figure S1B). The data collectively indicate that IL-4 induces early *Traf6* expression in a TGF-β-dependent manner, suggesting that TRAF6 expression might play a role in Th9 differentiation.

We next investigated whether Smad3 is involved in IL-4-and-TGF-β-induced TRAF6 expression. We cultured *Smad3* KO $CD4^+$ T cells with TCR stimulation in the presence of IL-4 and TGF-β and found that deletion of Smad3 completely blocked *Traf6* mRNA induced by IL-4 or IL-4 plus TGF-β (Figure 1C) and TRAF6 protein induced by IL-4 plus TGF-β (Figure 1D), suggesting a key role of Smad3 in this early TRAF6 induction.

We then studied which part of Smad3 protein activity was responsible for IL-4-plus-TGF-β-induced early expression of TRAF6 in $CD4^+$ T cells. As we recently reported that the phosphorylation of Smad3-Ser^{213}, rather than the phosphorylated Smad3 at C-terminal serine residues (p-Smad3C), is critical for *Il9* gene transcription,[5] we hypothesized that p-Smad3-Ser^{213} was also important for *Traf6* expression in response to IL-4 plus TGF-β. To address this, we generated Smad3 constructs that encoded a serine-to-alanine mutation at the linker region Ser213 site (Smad3-Ser^{213A}) or serine-to-alanine or threonine-to-valine mutations at all sites of the linker regions T179V, S204A, S208A, and S213A (EPSM)[5] (Figure S1C) and then transfected the indicated constructs or wild-type (WT) control construct into normal naive $CD4^+$ T cells (Figures 1E and 1F) or *Smad3* KO $CD4^+$ T cells (Figures 1G and 1H) followed by TGF-β and IL-4 stimulation for 2 h. Strikingly, normal or *Smad3* KO $CD4^+$ T cells that carried constructs with Smad3-Ser^{213A} alone or EPSM of Smad3 exhibited a profound decrease in *Traf6* mRNA (Figures 1E and 1G) and TRAF6 protein (Figures 1F and 1H) in response to IL-4 plus TGF-β stimulation, which corresponded to their respective reductions of IL-9 production in these mutated constructs as we previously found.[5] In addition, we showed that the blockade of p38 MAPK activity with its specific inhibitor SB203580 abolished TRAF6 protein expression in $CD4^+$ T cells stimulated with IL-4 plus TGF-β (Figure S1D), as phosphorylated p38 specifically induces Smad3-Ser^{213} phosphorylation.[5] In contrast, inhibition of either extracellular-signal-regulated kinase or c-Jun N-terminal kinase (JNK) phosphorylation with their individual inhibitors failed to change TRAF6 induced by IL-4 and TGF-β in $CD4^+$ T cells (Figure S1D). TRAF6-deficient T cells (*Traf6* KO mice, *Traf6*$^{f/f}$ CD4-cre$^+$ mice) abolished the IL-9 production induced by IL-4 plus TGF-β (Figures S1E and S1F). Although IL-6 plus TGF-β also induces IL-9 expression in $CD4^+$ T cells by activation of Stat6,[5] this combination of

stimuli was unable to increase TRAF6 (Figure S1G), suggesting the specific role of IL-4 plus TGF-β in TRAF6 expression. The data collectively provide compelling evidence that IL-4 plus TGF-β, through phosphorylation of Smad3-Ser^{213}, induces TRAF6, revealing a crosstalk between Smad3-canonical and -noncanonical pathways during Th9 differentiation.

IL-4 and TGF-β induce K63-linked Ub of TRAF6 by inhibiting NLRC3

The early upregulation of TRAF6 expression in response to IL-4 and TGF-β signaling encouraged us to study whether they also influenced the activity and function of TRAF6. It is known that the lysine 63 (K63)-linked polyubiquitination of TRAF6 is required to the activation of downstream pathways including TAK1,[6,20,21] which plays a critical role in the induction of the *Il9* gene in CD4$^+$ T cells.[4] In contrast, the type of polyubiquitin chains formed via K48 in TRAF6 normally targets it for proteasomal degradation.[21] Here, we found that IL-4 plus TGF-β caused TRAF6-Ub at the early time point (2 h) (Figure 2A) but clearly subsided after 4 h stimulation (Figure S2A). Stimulation of CD4$^+$ T cells with TCR in the presence of TGF-β failed to increase the total TRAF6-Ub compared to TCR stimulation alone (Figures 2A and 2B), and TCR plus IL-4 treatment induced a slight but inconsistent increase in TRAF6-Ub (Figures 2A and 2B). Of note, *Tgfbr1* KO CD4$^+$ T cells completely abolished the increase in TRAF6-Ub by IL-4 plus TGF-β stimulation (Figure 2A), suggesting an absolute requirement for TGF-β signaling in TRAF6-Ub. IL-4-plus-TGF-β-induced TRAF6-Ub also required Smad3, as *Smad3* KO T cells showed a complete failure of TRAF6-Ub in response to these two cytokines (Figure 2B). Thus, IL-4 plus TGF-β increases TRAF6-Ub in a TβRI-Smad3-signaling-dependent manner in addition to the induction of TRAF6 protein.

We next determined which polyubiquitin chain formed in TRAF6, i.e., via K48 or K63, was responsible for the activity of TRAF6 following IL-4 plus TGF-β stimulation, as these two types of Ub resulted in completely different fates of the TRAF6 function. We examined the TRAF6-Ub at K48 and K63 sites in T cells stimulated with IL-4 and TGF-β for 2 h (Figure 2C). The data showed that IL-4 alone substantially increased the TRAF6-Ub at K48 compared to T cells treated with TCR alone; IL-4-plus-TGF-β-treated cells, however, failed to further increase, and may have reduced, the TRAF6-Ub-K48 compared to IL-4 treatment alone (Figure 2C). In marked contrast, however, only IL-4 plus TGF-β, but not either one alone, substantially increased TRAF6-Ub-K63 (Figure 2C). Thus, IL-4 plus TGFβ induced TRAF6-Ub-K63 that mediates its activation, whereas IL-4 alone induces TRAF6-Ub-K48 that targets it for degradation.

To understand the molecular mechanisms by which IL-4 plus TGF-β activates TRAF6-Ub-K63 and IL-4 alone specifically induces TRAF6-Ub-K48, we examined the gene expression of leucine-rich-repeat-containing protein (NLRC3) and Numb-like protein (NUMBL) because NLRC3 prevents K63-linked Ub of TRAF6[22] and NUMBL promotes K48-linked Ub of TRAF6.[23,24] We found that by as early as 1 h, treatment of IL-4 plus TGF-β significantly decreased the expression of *Nlrc3* mRNA in T cells compared to T cells treated with medium, IL-4, or TGF-β alone (Figure 2D). In contrast, treatment of T cells with TGF-β plus IL-4 or either one alone did not significantly change *Numbl* expression (Figure 2E). The downregulated *Nlrc3* expression by TGF-β/IL-4 did not occur in the *Smad3* KO

cells (Figure S2B). The data indicate that IL-4-plus-TGF-β-induced K63 Ub of TRAF6 was primarily through inhibition of NLRC3 expression.

TRAF6-Ub-K63 activates TAK1 and NF-κB during Th9 differentiation

As TRAF6 E3 ligases plays a critical role in TAK1 activation via phosphorylation[6,25,26] and TAK1 is critical in *Il9* gene expression during Th9 differentiation,[4] we next investigated whether TRAF6-Ub-K63 activates TAK1 in response to IL-4 plus TGF-β. We firstly determined that IL-4 plus TGF-β indeed induced the TRAF6-TAK1 protein complex, indicating a direct protein-protein interaction, which was again completely abolished in T cells deficient in *Tgfbr1* (Figure 2A). Of note, IL-4 stimulation also formed a TRAF6-TAK1 complex in $CD4^+$ T cells (Figure 2A). However, IL-4 plus TGF-β, but not either one alone, induced substantial activation of TAK1 determined by increased p-TAK1, which was again abolished in *Tgfbr1* KO T cells (Figure 2F). The interaction of TRAF6-TAK1 also disappeared after 4 h stimulation (Figure S2A).

TRAF6 activation is a key step in NF-κB activation in Th9 cells.[21,26–28] To confirm NF-κB activation by TAK1 during Th9 cell differentiation, we firstly examined the activation of NF-κB signaling and found that IL-4 plus TGF-β induced the phosphorylation of NF-κB p65 and p-IκBα (Figure 2G), as well as the p65 nuclear localization at 4 h (Figure 2H). Strikingly, either deletion of *Traf6* in T cells (Figure S2C) and blockade of TAK1 activity with its specific inhibitor (5z-7-oxozeaenol) (Figure S2D) significantly decreased NF-κB p65 activation compared to control cells. Consistently, inhibition of TAK1 or p65 substantially reduced Th9 cells induced by IL-4 and TGF-β (Figures 2I and 2J). Thus, TAK1-NF-κB signaling is activated by TRAF6-Ub-K63 and promotes Th9 differentiation.

TRAF6-TAK1-NF-κB axis downregulates E2f8 expression during Th9 differentiation

As p-Smad3-Ser^{213} is not only required for the expression of TRAF6 (Figures 1E–1H) but also regulates the expression of transcription factors DBP (as an activator) and E2f8 (as a repressor) in regulating *Il9* gene transcription in response to IL-4 plus TGF-β,[5] we hypothesized that the TRAF6-TAK1-NF-κB axis was involved in DBP and E2f8 expression. To test this, we firstly showed that the deficiency of TRAF6 significantly downregulated *Il9* gene transcription (Figure 3A). Interestingly, the increased mRNA and protein of DBP in WT $CD4^+$ T cells by IL-4 plus TGF-β stimulation were significantly downregulated in *Traf6* KO cells (Figures 3B, left, and 3C). On the other hand, the decrease in the mRNA and protein of E2f8 by IL-4 plus TGF-β treatment in WT T cells was completely reversed in *Traf6* KO T cells (Figures 3B, right, and 3C), indicating a key regulatory role of TRAF6 in DBP and E2f8 expression.

As TAK1 is activated by TRAF6-Ub-K63 in $CD4^+$ T cells and activated TAK1 is required for IL-9 production in response to IL-4 plus TGF-β stimulation (Figure 2), we next investigated the function of TAK1 in DBP and E2f8 expression during Th9 differentiation. Consistent with our previous findings,[4] blockade of TAK1 activity markedly reduced the *Il9* gene transcription (Figure 3D). Strikingly, TAK1 inhibition significantly decreased the expression of *Dbp* gene but upregulated *E2f8* gene expression in $CD4^+$ T cells in response to IL-4 plus TGF-β (Figure 3E). Consistently, TAK1 inhibition also substantially decreased

the amounts of DBP protein but increased E2f8 protein during IL-4 plus TGF-β stimulation (Figure 3F).

We next determined the role of NF-κB p65 in the regulation of DBP and E2f8 during *Il9* gene transcription. $CD4^+$ T cells that were treated with p65 inhibitor and then stimulated with IL-4 plus TGF-β failed to transcribe *Il9* (Figure 3G). Importantly, the inhibition of p65 completely reversed the downregulated expression of the mRNA and protein of E2f8 induced by IL-4 plus TGF-β but, unexpectedly, did not affect the expression of *Dbp* mRNA and DBP protein in $CD4^+$ T cells (Figures 3H and 3I). Thus, we have established that the TRAF6-TAK1-NF-κB p65 axis specifically regulates the expression of E2f8, which controls *Il9* gene transcription in response to IL-4 plus TGF-β during Th9 differentiation.

Identification of *miR-19b* as direct inhibitor to E2f8 in Th9 differentiation

As miRNA has been reported in regulating T cell differentiation, we next investigated whether miRNA was involved in Th9 differentiation and whether it required the TRAF6-TAK1-NF-κB p65 axis in response to IL-4 plus TGF-β signaling. For this, we first profiled the miRNA assay using the nCounter miRNA expression analysis system workflow for naive $CD4^+$ T cells under the four culture conditions: medium (control), IL-4, TGF-β, and IL-4 plus TGF-β at 24 h. We found that 11 miRNAs significantly increased in IL-4-treated cells compared with control cells ($p < 0.05$, fold change > 2) (Figure S3A). Among them, *miR-19b* (fold change = 3.67) and *miR467f* (fold change = 3.58) were enhanced in IL-4-plus-TGF-β-treated cells compared with medium control cells (Figure S3A). Interestingly, TGF-β treatment alone did not increase any miRNA compared to medium-treated control (Figure S3B). Among all miRNAs that increased in IL-4-treated cells, *miR-19b* showed the highest upregulation under Th9 conditions, suggesting that *miR-19b* may play a critical role in Th9 cell differentiation. Consistently, the increase in *miR-19b* was validated by real-time PCR at 24 h after IL-4 plus TGF-β stimulation in $CD4^+$ T cells (Figures 4A and S3C). Importantly, the expression of *miR-19b* induced by IL-4 and TGF-β was suppressed in *Tgfbr1* KO (Figure 4B), *Smad3* KO (Figure 4C), and *Traf6* KO (Figure 4D) T cells, as well as in TAK1- and p65-inhibited WT T cells (Figure 4E), suggesting a required role of the TRAF6-TAK1-NF-κB p65 axis in *miR-19b* induction.

To confirm the role of *miR-19b* during Th9 cell differentiation, $CD4^+$ T cells were transfected with *miR-19b* mimic or treated with *miR-19b* inhibitor, respectively. Overexpression of *miR-19b* increased the expression of *Il9* mRNA and IL-9 protein in $CD4^+$ T cells induced by IL-4 plus TGF-β (Figures 4F, 4H, and S3D), but inhibition of *miR-19b* downregulated *Il9* mRNA and IL-9 protein levels (Figures 4G, 4H, and S3D), suggesting that *miR-19b* is a key regulator for Th9 differentiation.

To understand the downstream transcription factors to which *miR-19b* targets in *Il9* gene expression, we identified that the *E2f8* gene is one of the predicted targets of *miR-19b* by using the miRDB, TargetScan, and StarMirDB databases (Figure S3E). To determine whether *miR-19b* is involved in the downregulation of E2f8, we investigated the expression of the mRNA and protein of E2f8 in *miR-19b*-overexpressed or -inhibited T cells followed by IL-4 and TGF-β treatment. We discovered that overexpression of *miR-19b* resulted in a significant reduction in E2f8 compared to control mimic cells (Figure 4I), but the reduction

of *miR-19b* significantly increased E2f8 compared to control inhibitor-treated cells (Figure 4J).

To further validate the direct binding of *miR-19b* in *E2f8* mRNA for Th9 differentiation, we constructed plasmids with the *E2f8* 3′ UTR, including the WT sequence and mutated sequence at the binding sites of *miR-19b* (Figure S3F), and performed the luciferase reporter assay. Overexpression of *miR-19b* suppressed luciferase activity driven by the *E2f8* 3′ UTR WT construct, while the mutant construct was unresponsive to *miR-19b* overexpression (Figure 4K), suggesting that *miR-19b* directly binds to the 3′ UTR of *E2f8*. Surprisingly, *miR-19b* expression was increased only in IL-4-plus-TGF-β-mediated Th9 cells (Figure S3G) but no other T cell subsets, including Th1, Th2, Th17, and Treg cells, compared to Th0 cells. However, the *miR-467f* increase was not exclusive to Th9 cells but could also be significantly upregulated in Treg cells and Th17 cells (Figure S3H). Furthermore, the overexpression of *miR-467f* does not affect IL-9 production in IL-4-plus-TGF-β-stimulated T cells (Figure S3I), excluding *miR-467f*'s involvement in Th9 cell differentiation. The data collectively indicate that *miR-19b* expression downstream of TRAF6-TAK1-NF-κB p65 signaling downregulates *E2f8* to activate Il9 gene.

A key role of *miR-19b*-mediated Th9 cells in SSc

It has been reported that IL-4, TGF-β, and IL-9 are elevated in patients with SSc,[29–31] but the mechanisms by which Th9 cells are differentiated in SSc and the causative effects of Th9 cells on the development and pathogenesis of SSc remain poorly defined. Having established the role of *miR-19b* in regulating IL-9 production in Th9 cells *in vitro*, we next determined the function of *miR-19b*-mediated Th9 cells in the SSc mouse model *in vivo*. Firstly, we investigated the IL-9 function in the bleomycin (BLM)-injected SSc mice model, which exhibited skin and pulmonary inflammation and fibrosis that resemble many key features of patients with SSc. We treated the SSc mice with anti-IL-9 neutralizing antibody or control immunoglobulin G (IgG) (Figure 5A) and found that mice injected with anti-IL-9 exhibited significantly suppressed BLM-induced scleroderma quantified by measuring the dermal thickness of the ears and back skin at the injection site, which was accompanied by significantly less body weight loss compared with the BLM-injected group receiving the control antibody (Figures 5B–5D). Consistently, histopathological changes by H&E staining and collagen deposition by Masson's trichrome staining in the skins were substantially improved in anti-IL-9-treated SSc mice compared to the control IgG-injected SSc group (Figure 5E). The dermal thickness from skin biopsies in Figure 5E was also significantly lower in the anti-IL-9-treated group than the control IgG-injected group, which was actually comparable with that in saline-injected healthy control mice (Figure 5F). Similar to the histological evaluation of skin sections, BLM-induced lung injury was also attenuated by anti-IL-9 injection (Figure 5G). The data indicate that IL-9 plays a key role in the development and pathogenesis of SSc.

We next analyzed gene expression in $CD4^+$ T cells isolated from the SSc mice. We showed that the mRNA expression of *Il9* and *miR-19b* in T cells was significantly increased in BLM-induced SSc mice, which was significantly reduced by anti-IL-9 antibody treatment (Figures 5H and 5I). BLM-induced SSc mice had a marked reduction of the *E2f8* gene in

$CD4^+$ T cells compared with those from saline-injected healthy control mice (Figure 5J), but anti-IL-9-treated SSc mice showed no difference of *E2f8* gene expression compared to control-IgG treated SSC mice, consistent with the fact that *Il9* is the downstream target of *E2f8*.[5] The expressions of profibrogenic genes such as *Acta2, Col1a1, Col1a2, Mmp2, Fn1*, and *Vmac* were markedly decreased in anti-IL-9-treated mice compared to untreated and control antibody-treated SSc mice (Figures 5K and 5L).

Next, we determined the function of *miR-19b* in the BLM-induced SSc model with an *miR-19b* inhibitor (Figure 6A). Notably, administration of the *miR-19b* inhibitor significantly suppressed the disease of SSc with a decrease in the dermal thickness of the ears and skin and recovery of weight loss compared to control inhibitor-injected SSc mice (Figures 6B–6D). Consistently, *miR-19b* inhibition alleviated histopathological changes and collagen deposition in the skin and lungs of SSc mice (Figures 6E–6G). Consistent with the *in vitro* results shown in Figures 4G and 4J, the expressions of *Il9* and *miR-19b* mRNA in $CD4^+$ T cells were reduced in *miR-19b*-inhibitor-injected SSc mice compared with the control inhibitor-treated SSc group (Figures 6H and 6I), and the reduction of *Il9* was due to *miR-19b*-inhibition-mediated upregulation of *E2f8* expression in the SSc mice (Figure 6J). In addition, *miR-19b* blockade in SSc mice significantly suppressed the serum levels of IL-9 (Figure 6K). The expression of the *Il9* gene in the skin and lung tissues was significantly suppressed in the miR-19b-inhibited SSc group compared with the control group (Figures 6L and 6M), further validating the role of *miR-19b* in promoting Il9 gene expression.

Importantly, we observed that the profibrogenic genes were significantly suppressed in the skin from the *miR-19b*-inhibited SSc group (Figure S4A) and also reduced by a similar trend in the lungs (Figure S4B), suggesting an amelioration of fibrogenesis by *miR-19b* inhibition in the BLM-induced SSc mouse model in vivo. We evaluated the frequencies of interferon (IFN)-γ-, IL-4-, IL-10-, IL-13-, IL-17a-, and Foxp3-producing $CD4^+$ T cells from the lungs and spleens (Figures S4C and S4D) among all the groups of mice. No significant changes were found for each individual cytokine between the SSc mice treated with the *miR-19b* inhibitor and untreated SSc mice (Figures S4C and S4D). Taken all together, we have revealed that *miR-19b*-mediated Th9 cells play a crucial role in the pathogenic development of SSc in mice.

Th9 cells promote pulmonary fibroblast-to-myofibroblast transition *in vitro*

To understand the mechanisms by which Th9 cells exacerbate SSc, we investigated whether Th9 cells exert profibrotic effects. For this, we first prepared primary fibroblasts from the mouse lungs (Figure S5A), confirmed the increased mRNA and protein levels of α-smooth muscle actin as a key marker of myofibroblast differentiation, and showed that IL-9 treatment activated myofibroblast differentiation from fibroblasts in a dose-dependent manner (Figures S5B and S5C). The fibroblasts treated with IL-9 for 24 h showed the expression of fibrogenic genes including *Acta2, Col1a1, Mmp2*, and *Mmp9* (Figure S5D). Furthermore, we found higher expression of fibrogenic markers in fibroblasts that were cocultured with Th9 cells than naive $CD4^+$ T cells (Th0), and the increase was reversed when IL-9 was blocked by anti-IL-9 antibody (Figure S5E). Importantly, as observed in SSc mice injected with the *miR-19b* inhibitor, primary fibroblasts that were cocultured with

miR-19b-preinhibited Th9 cells exhibited significantly lower expression of fibrogenic genes (Figure S5F). These findings reveal the profibrotic effect of Th9 cells that are controlled by *miR-19b*.

MIR-19B-associated TH9 cells in patients with SSc

Next, we collected naive human $CD4^+$ T cells isolated from peripheral blood mononuclear cells and then examined the IL-9-producing TH9 cells by TGF-β and IL-4 stimulation for 5 and 8 days (Figure S6). Consistent with mouse $CD4^+$ T cells, human $CD4^+$ T cells can also promote the activation of TRAF6 and TAK1 in response to TGF-β and IL-4 combination treatment (Figure 7A). Overexpression of *MIR-19B* markedly increased *IL9* gene expression in human $CD4^+$ T cells compared to controls (Figure 7B), while inhibition of *MIR-19B* suppressed *IL9* gene expression (Figure 7C). We next extend our studies to investigate the clinical significance of the expression of *MIR-19B* and TH9 cells in patients with SSc. As expected and consistent with our findings in the SSc mouse model, we observed that the circulating level of IL-9 protein was higher in the blood of patients with SSc compared to healthy control subjects (Figure 7D). *IL9* mRNA in $CD4^+$ T cells of the patients also exhibited an increase compared with healthy controls (Figure 7E). The same $CD4^+$ T cells in the patients also increased *MIR-19B* expression (Figure 7F). When analyzing the expression of each gene related to the worsening of the modified Rodnan skin score (mRSS) as an indicator of disease progression, we found that patients with higher mRNA levels of *IL9* and *MIR-19B* had a worse mRSS (Figures 7G and 7H). Furthermore, *IL9* and *MIR-19B* showed a strongly positive relationship in $CD4^+$ T cells from the patients with SSc (Figure 7I). Thus, *MIR-19B*-driven TH9 cells are also involved in the pathogenesis of human SSc.

DISCUSSION

In this study, we have discovered that Th9 cells play a key role in the development and pathogenesis of SSc and that *miR-19b* drives Th9 differentiation to promote the exacerbation of SSc. Mechanistically, we have elucidated that *miR-19b* is induced through the activation of the TRAF6-TAK1-NF-κB p65 axis downstream of TβRI-Smad3-Ser^{213} signaling in response to TGF-β plus IL-4 signaling. *miR-19b*, in turn, activates the *Il9* gene by inhibition of the transcription factor E2f8, a repressor for *Il9* gene transcription.[5] Importantly, we found that Th9 cells driven by *MIR-19B* are also associated with pathogenesis in patients with SSc.

TAK1 plays a positive role in *Il9* gene expression and Th9 differentiation in response to TGF-β plus IL-4.[4] As TAK1 is activated via its upstream transcription factor TRAF6, which represents a noncanonical pathway in transducing TGF-β signaling by TβRI-mediated p38/JNK activation,[7] it is important to understand the role of TRAF6 in bridging TGF-β signaling to the activation of TAK1 during Th9 differentiation. Notably, we have recently demonstrated that activated p38-mediated p-Smad3-Ser^{213}, but not p-Smad3C, is required for *Il9* gene activation by TβRI-dependent signaling during TGF-β and IL-4 stimulation.[5] We thus hypothesized that TRAF6 could be the missing link in connecting the Smad3-dependent pathway to the TAK1-dependent noncanonical pathway for Th9 differentiation.

Indeed, we discovered that the induction and activation of TRAF6 is an early and essential step in the cascade for *Il9* gene activation in $CD4^+$ T cells in response to TGF-β plus IL-4. Previous studies suggested that TRAF6 is involved in amplifying the signaling downstream of OX40 to enhance Th9 proliferation,[8,32] but whether TRAF6 is required for initiation downstream of TGF-β plus IL-4 signaling was not known. We uncovered here that IL-4 signaling induces a rapid and early expression of *Traf6* mRNA (2 h), which is paradoxically dependent on TGF-β signaling, as *Tgfbr1* KO T cells fail to express Traf6 in response to IL-4 stimulation. Even more surprisingly, despite Traf6 mRNA expression being induced by IL-4 alone, only the combinatory signaling of TGF-β plus IL-4 could increase TRAF6 protein. This suggests that IL-4 signaling is critical in detouring the classic TGF-β pathway by inducing *Traf6* mRNA to initiate the cascade of molecular programs to activate the *Il9* gene, as opposed to other programs such as Foxp3 and Il17 gene activation that also require TGF-β signaling. However, IL-4 signaling alone is insufficient to accomplish the program without TGF-β signaling, as evidenced by its inability to translate the mRNA into the protein of TRAF6, although how it is achieved remains unknown. Nevertheless, TRAF6 protein expression was abolished by blockade of p38 MAPK activity in normal T cells or T cells with a mutation of Smad3-Ser^{213A}, indicating that TRAF6 expression is regulated by p38-Smad3-Ser^{213} signaling cascades during Th9 conditions.

The activation of TRAF6 protein is through its Ub, and it is known that K48-linked polyubiquitination of TRAF6 targets proteins for degradation, but K63 polyubiquitination acts as a scaffold to assemble protein kinase complexes and mediate their activation.[25] TRAF6 autoubiquitination is frequently utilized as an indicator of TRAF6 activation in immune cells, including T cells, B cells, and myeloid cells.[21] We found that IL-4 alone and IL-4 plus TGF-β treatments increase the K48-linked Ub of TRAF6; however, only IL-4 plus TGF-β stimulation promotes K63-linked Ub. This result is attributed to the downregulation of *Nlrc3* expression because NLRC3 decreases the K63-linked Ub of TRAF6.[22] These data explain why IL-4 alone can induce *Traf6* mRNA but is unable to promote Th9 differentiation, as IL-4 fails to induce functional K63-linked Ub of TRAF6. In fact, K63-linked Ub of TRAF6 thus allows target activation such as TAK1,[6,21,25] and also, the ubiquitinated TRAF6 positively regulates NF-κB signaling activation in $CD4^+$ T cell subsets.[27] In this study, we confirmed here that TRAF6 K63 Ub is essential for TAK1 activation and NF-κB cascade signaling during Th9 cell differentiation, thus establishing TRAF6-TAK1-NF-κB axis involvement downstream of Smad3-Ser^{213} signaling required for *Il9* gene expression. Previously, it was reported that OX40 engagement directly activates *Il9* gene transcription through the TRAF6-NF-κB signaling pathway.[32] However, it is unlikely that OX40 signaling is related to p-$Smad3^{Ser213}$-mediated TRAF6 activation in TGF-β/IL-4-differentiated Th9 conditions. Although the underlying mechanism for these differences remains unknown, our finding does not preclude a role for OX40 in IL-9 production through other pathways.

In addition, consistent with the data that TRAF6 deficiency in $CD4^+$ T cells dramatically suppressed *Il9* and *miR-19b in vitro*, $Traf6^{f/f}$ CD4-cre^+ SSc mice also show a decrease in skin thickness, albeit with no difference in the changes of body weight, compared to WT mice *in vivo*. Analysis of the $CD4^+$ T cells isolated from the $Traf6^{f/f}$ CD4-cre^+ SSc mice revealed that the KO $CD4^+$ T cells exhibited reduced *Il9* and *miR-19b* expression.

Recently, we have reported that transcription factors DBP and E2f8 act as an activator and a repressor, respectively, for *Il9* gene expression, and especially, the suppression of E2f8 is specific in Th9 cell differentiation.[5] However, the mechanism of E2f8 suppression and the specific regulatory factors involved in its modulation have not been elucidated. In most cases, the translation initiation and stability of target genes is inhibited by miRNAs, and each protein-coding gene can be regulated by several miRNAs.[12] Consistent with this notion, we hypothesized that E2f8 may be regulated by miRNA in Th9 cell differentiation. Indeed, we have identified here through miRNA analysis that *miR-19b* and *miR-467f* are highly expressed during Th9 differentiation induced by IL-4 plus TGF-β. It was recently demonstrated that *miR-467f* can inhibit the expression of proinflammatory cytokines including TNF and IL-1β by downregulation of *Map3k8*, which is upstream of the p38 MAPK signaling pathway in microglia isolated from a murine amyotrophic lateral sclerosis model.[33] We have, however, discovered that the expression of *miR-467f* is not exclusive to Th9 cells but can also be upregulated in other Th subsets, including Th17 and Treg cells. Importantly, we found, through gain- and loss-of-function studies, that *miR-467f* does not affect IL-9 production induced by IL-4 and TGF-β stimulation, thus eliminating *miR-467f* as a player in Th9 differentiation.

Instead, we have discovered that *miR-19b* is the key miRNA regulating Th9 differentiation. *miR-19b* was identified as an oncogenic component of the *miR-17–92* cluster, which encodes *miR-17, miR-18a, miR-19a, miR-20a, miR-19b-1*, and *miR-92a-1*.[34] In cancers, *miR-19b-3p* plays a critical role to promote cell proliferation, invasion, and metastasis in non-small cell lung cancer,[35] esophageal squamous cell carcinoma,[36] and gastric cancer cells.[37] *miR-19b* is also reported to play a role in enhancing Th1[16] and Th17[18] proliferation while preventing inducible Treg differentiation by targeting the tumor-suppressor protein PTEN.[16] In asthma, *miR-19b* promotes Th2 cytokines, such as IL-13 and IL-4, from T cells via the direct targeting of PTEN, SOCS1, and A20.[17] However, these genes predicted to be targeted by *miR-19* in T cells were not involved in the IL-4 and TGF-β signaling pathway under our Th9 conditions. Additionally, in our previous paper,[5] we identified several potential factors for regulating *Il9* transcription using analysis of motif enrichment. Among them, E2f8, Stat5b, and Nfatc2 were predicted to be targeted by *miR-19*; however, we found that only E2f8 was negatively regulated during TGF-β/IL-4-Th9 cell differentiation. Importantly, *E2f8* is a target gene of *miR-19b*, as inhibition of *miR-19b* reverses the downregulation of E2f8 and, consequently, blocks *Il9* gene transcription during Th9 cell differentiation. Conversely, overexpression of *miR-19b* in $CD4^+$ T cells through *miR-19b* mimic transfection enhances IL-9 cytokine production, while other major cytokines such as IFN-γ and IL-17, as well as the expression of Foxp3, remain unaffected. Simultaneously, this overexpression also led to a slight increase of IL-4 production,[17] which could provide a positive feedback mechanism to amplify Th9 differentiation. Furthermore, we identified that *miR-19b* can bind directly to the *E2f8* 3′ UTR by luciferase reporter assay. This establishes the basis for *miR-19b*-specific regulation of Th9 cells. Nevertheless, there is a possibility of other targets regulated by *miR-19b* contributing to Th9 differentiation.

Typically, transcription factors work upstream of miRNAs, while concurrently, miRNAs control the expression of target mRNA, including the transcription factors.[38] Given that transcription factor NF-κB plays a critical role in regulating the expression of miRNAs that

include *miR-30b*,[39] *miR-125b*,[40] *miR-146a*,[41,42] and *miR-155*[42,43] in the immune system, we hypothesized that NF-κB might be implicated in the expression of *miR-19b* under our Th9 conditions. We confirmed that NF-κB p65 can be rapidly induced by TGF-β and IL-4, and the inhibition of NF-κB p65 by its specific inhibitor leads to decreased *miR-19b* and increased E2f8 expression. Furthermore, we have demonstrated the function of TRAF6 and TAK1 in *miR-19b* expression, supporting our notion that the expression of *miR-19b* is dependent on the activation of the TRAF6-TAK1-NF-κB axis in response to IL-4 and TGF-β signaling.

Recently, studies have shown that systemic IL-9 is increased in the skin, kidney, and peripheral blood of patients with SSc.[29,44] However, the exact molecular mechanisms underlying IL-9 production and function in SSc remain unknown. Here, we have revealed that the regulatory role of *miR-19b* in Th9 cells contributes to Th9-mediated pathogenesis of SSc in a mouse model *in vivo*. Evidence supporting this conclusion includes that both *miR-19b* expression and IL-9 production in $CD4^+$ T cells are increased in BLM-induced SSc mice and the increase in IL-9 exacerbates fibrogenesis and myofibroblast differentiation in skin and lung tissue, as neutralization of IL-9 with antibody suppresses the pathogenesis of SSc evidenced by the reduction of key genes in SSc, including *Acta2, Col1a, Col1a2, Mmp2*, and *Fn1*. Importantly, *miR-19b* inhibition in the BLM-induced SSc mouse model significantly suppressed profibrogenic genes, which is likely due to the reduction of circulating IL-9 and tissue-specific IL-9 in the skin and lungs. This is ascribed to the inhibition of Th9 cell differentiation caused by increased *E2f8*.

Th9 cells are relatively new and less well characterized compared to other T cell subsets. Additionally, there remain challenges in understanding how Th9 cells are induced and what their functions are *in vivo*. Thus, we have tried to figure out the roles of Th9 cells in various disease models, recognizing that it can be multifaceted depending on the disease settings. Previously, we showed successfully that Th9 cells are involved in the suppression of tumor growth in tumor models. However, in those tumor models, we used the adoptive transfer of *in-vitro*-differentiated Th9 cells into tumor mice, which are not ideal models to test the function of the *miR-19b*-Th9 pathway *in vivo*. We have also tried to explore the function of Th9 cells in experimental asthma and experimental autoimmune encephalomyelitis (EAE) models, but unfortunately, we did not observe any significant roles of Th9 in the pathogenesis of these two models. Thus, we did not use these models to test the function of *miR-19b in vivo*. Although there is a limitation in using only an SSc mice model, we believe that this model is, so far, the best model to test this *miR-19b*-Th9 function *in vivo*. More importantly, we observed that the levels of *IL9* and *MIR-19B* in patients with SSc increased and are correlated with scleroderma in patients, validating the clinical significance of the findings in the experimental SSc and clarifying the role of *MIR-19B* as a valuable factor for evaluating disease progression. The findings provide *MIR-19B* as a biomarker and potential target for the investigation of TH9-associated pathogenesis in human autoimmune diseases such as SSc and beyond.

Limitation of the study

Our study has limitations regarding data collection, analysis, and interpretation from patients with SSc. We plan to expand the number of patients to further validate our findings and elucidate the mechanisms underlying *MIR-19B* and IL-9/TH9 in the pathogenesis of patients with SSc. In the present study, we used $CD4^+$ T cells isolated from the peripheral blood of the patients and demonstrated a relationship between *MIR-19B* expression in T cells and disease progression by measuring the worsening of the mRSS. However, as reported in the literature, IL-9-producing Th9 cells were hardly detectable in the tissues of the experimental mouse disease models, including SSc. Therefore, there are still challenges in understanding how Th9 cells function under various *in vivo* conditions. Therefore, we are striving to elucidate the roles of *miR-19b* in Th9 cells in other disease models, recognizing that it could be multifaceted depending on the disease settings.

STAR★METHODS

RESOURCE AVAILABILITY

Lead contact—Further information and requests for resources and reagents should be directed to and will be fulfilled by the lead contact, WanJun Chen (wchen@nih.gov).

Materials availability—Any plasmids generated in this study are available from the lead contact; however, we may require a completed materials transfer agreement.

Data and code availability

- Raw miRNA-seq data reported in this paper have been deposited in the GEO database under accession number listed in the key resources table.
- This paper does not report original code.
- Any additional information required to reanalyze the data reported in this paper is available from the lead contact upon request.

EXPERIMENTAL MODEL AND STUDY PARTICIPANT DETAILS

Mice—Male and female C57BL/6 mice were obtained from The Jackson Laboratory. *Tgfbr1*$^{f/f}$ -ER^{cre}, *Traf6*$^{f/f}$ -CD4^{cre} and *Smad3* KO mice (on a C57BL/6 background) were housed and generated in the animal facility in National Institute of Dental and Craniofacial Research (NIDCR). Both sexes in the age of 8–10 weeks were used for all experiments. All mice were co-bred under the same conditions in a 12 h light/dark cycle-, temperature (23 ± 3°C)- and humidity (range 40–60)-controlled room. All animal studies were performed according to US National Institutes of Health (NIH) guidelines for the use and care of live animals and approved by the Animal Care and Use Committees (ACUC) of NIDCR.

Murine and human primary T cell isolation and culture—Spleen and lymph nodes were isolated from mouse, and red blood cells (RBC) were removed by ACK buffer. Naive $CD4^+$ T cells were purified by MACS magnetic bead cell sorting and were cultured with plate-bound anti-mouse CD3 (1 μg/mL) plus soluble anti-mouse CD28 (1 μg/mL). Human $CD4^+$ T cells isolated from PBMCs provided by healthy volunteers were obtained from the

Department of Transfusion Medicine (DTM) of the NIH (NCT000001846). The isolated cells were cultured with plate-bound anti-human CD3 (1 μg/mL) and soluble anti-human CD28 (1 μg/mL). These cells were incubated with a combination of TGF-β1 (2 ng/mL) and IL-4 (10 ng/mL) for Th9 differentiation.

Murine pulmonary fibroblasts isolation and coculture with T cells—We collected the lungs from WT mouse and made a small incision with surgical scissors. For the enzymatic digestion, we incubated the tissue at 37°C for 30 min in 1 mg/mL Collagenase/Dispase digestion buffer, and then minced the digested lung to generate a single-cell suspension. They were cultured with DMEM media supplemented with 10% FBS, which can be maintained for up to 5 passages, we used a maximum of 3 passages. For coculture with $CD4^+$ T cells, the primary fibroblasts (3×10^4 cells) were plated in 12-well culture plates and activated T cells were added directly to the plates at a fibroblast/T cell ratio of 1:5.

Bleomycin-induced SSc mouse model—8-week-old mice were injected daily Bleomycin subcutaneously (1 mg/kg/day) using 27-gauge needle for 28 days. Control mice received injections of 100 μL PBS. For *in vivo* neutralization of IL-9 after Bleomycin injection, mice were treated intraperitoneally with 100 μg anti-IL-9 antibody or mouse anti-IgG2a isotype control every three days. Injection of MiRCURY LNA *miR-19b-3p* inhibitor (200 μg) or control inhibitor was performed on the 1, 3, 5, 15, 17, and 19^{th} days (6 times). Body weight was measured using a digital scale every 2 or 3 days. The mice were sacrificed on day 28. We measured the skin thickness in two perpendicular dimensions with calipers and collected the skin and lung tissues to analyze the change in the local milieu.

Patients—The study was approved by the Drum Tower Hospital Ethics Committee (2008017). Blood samples from the patients with SSc and healthy individuals were collected from the Affiliated Drum Tower Hospital of Nanjing University Medical School in China. Peripheral blood $CD4^+$ $CD45RA^+$ T cells from the patients with SSc and healthy controls were isolated to identify the expression of *IL9* and *MIR-19B*. All patients met the American College of Rheumatology/European League Against Rheumatism 2013 classification criteria for SSc[45] and signed the informed consent form with full notification. Healthy controls (HC) were recruited at the Health Examination Center of the same hospital upon written informed consent. The modified Rodnan Skin Score (mRSS) for each enrolled patient was measured by the same investigator, by estimating skin thickness using a 0–3 scale in 17 body areas.[46] See Table S1 for more information.

METHOD DETAILS

Real-time RT-PCR—Total RNA was derived from cultured cells with an RNeasy Mini kit, and cDNA was synthesized with a High Capacity cDNA Reverse Transcription kit. Quantitative real-time PCR was performed according to the protocol of TaqMan gene expression master mix using QuantStudio 3. To enhance cDNA and detect the amount of miRNAs, we used TagMan Advanced miRNA cDNA Synthesis Kit. Real-Time PCR Systems (Applied Biosystems) with primers. Results were normalized to those of *Hprt* mRNA. The *miR-19b* expression was determined relative to internal *U6* small nuclear RNA

in T cells or calculated using exogenous *cel-miR-39* as reference controls for serum miRNA normalization. All data were quantified by the $2^{-\Delta\Delta CT}$ method.

miRNA microarray and analysis—Total RNA samples were profiled by nCounter mouse v1.5 miRNA Expression Assay Kit. The expressed data were normalized using the median normalization analysis. Statistically significant differentially expressed microRNAs were defined as $p < 0.05$ and fold change >2. Scanned images were imported into GenePix Pro 6.0 (Axon) for grid alignment and data extraction.

Bioinformatics analysis—Identification of the putative *miR-19b-3p* target genes was performed using miRDB, TargetScan and STarMirDB.

Retroviral production and transduction—Myc-DDK-tagged E2f8 was amplified and subcloned into pMSCV-IRES-GFP retroviral vector (Addgene) using *XhoI* restriction enzyme. E2f8 mutant plasmid of *miR-19b* binding region was obtained from WT E2f8 construct using QuikChange II Site-Directed Mutagenesis kit according to the manufacturer's instructions. For luciferase reporter assay, the WT or mutant *E2f8* 3′UTR for the *miR-19b* binding sites were cloned into the *Xho*I and *Xba*I sites of pmirGLO Dual-Luciferase miRNA Target Expression Vector from GenScript. For recombinant retroviral production, human embryonic kidney (HEK) 293 T cells were transiently transfected with the E2f8 vector and pCL-ECO packaging vector using TurboFect transfection reagent. After 48 h post-transfection, the culture supernatant containing viruses was collected and filtered.

Transfection—$CD4^+$ T cells stimulated with anti-CD3 and anti-CD28 were spinfected with viral supernatant supplemented with polybrene (5 μg/mL). The medium was replaced with fresh medium, and these cells were cultured for an additional 48 h in complete cell culture medium. $CD4^+$ T cells were transfected with 200 nM miRNA inhibitor or 50 nM miRNA mimic using Lipofectimine RNAiMAX for 24 h according to the manufacturer's instructions. The performance of each miRNA inhibitor or mimic was compared to its negative control, which was purchased from the same supplier.

Flow cytometry—For intracellular cytokine staining, the cells were stimulated for 4 h at 37°C with PMA (phorbol 12-myristate 13-acetate; 10 ng/mL), ionomycin (1 μg/mL) and GolgiPlug (1:1,000 dilution) and fixed with Fixation/Permeabilization buffer solution or Foxp3/Transcription Factor Staining Buffer Set. The cells were incubated with fluorochrome-conjugated antibodies (all diluted 1:100) in FACS buffer (0.5% BSA and 0.1% NaN_3 in PBS) for 30 min. For detecting cytokine expression in tissues harvested from SSc mice model, single-cell suspensions were prepared. In brief, skin and lung tissues were cut into small pieces and digested with 4 mg/mL collagenase IV and 1 mg/mL DNase I at 37 for 1 h. Cell suspensions were washed by FACS buffer and passed through 40 μm cell strainers. Flow cytometry was performed on a FACS Fortessa and analyzed with FlowJo software v 10.7.1.

Western immunoblotting and immunoprecipitation—The proteins samples were extracted with RIPA lysis buffer. For detection of TRAF6 ubiquitination, lysates were immunoprecipitated with anti-TRAF6, followed by immunoblotting with anti-Ubiquitin.

They were separated by SDS-PAGE and transferred onto polyvinylidene difluoride (PVDF) membranes (Milipore). The membranes were blocked with 5% nonfat milk in TBST (0.5 M NaCl, Tris-HCl, pH 7.5 and 0.5% Tween 20) for 1 h at room temperature and separately incubated with the primary antibodies (all antibodies used at a dilution of 1:1000) in 5% BSA in TBST overnight at 4°C. The membranes were washed with TBST buffer and then incubated with horseradish peroxidase-conjugated secondary antibodies (1:2000 dilution) for 1 h. The results were visualized by enhanced chemiluminescence according to the manufacturer's protocol.

ELISA—For IL-9 cytokine assays, the cell culture supernatants were collected after 72 h. Cytokine was quantified using IL-9 ELISA kit according to the manufacturer's protocol.

Luciferase assay—The HEK 293 T cells were co-transfected with *E2f8* WT or mutant-binding element together with the control or *miR-19b* mimic, respectively. After 24 h transfection, we performed luciferase assay using Dual-Luciferase reporter assay system, according to the manufacturer's instructions.

Histological analysis—Skin and lung tissues of Bleomycin-induced SSc mouse model were harvested for staining with hematoxylin and eosin (H&E) or Masson's trichrome stains. Skin samples were collected near the injection site of Bleomycin. For Masson's trichrome staining, the skin and lung tissues were perfused and fixed with 4% paraformaldehyde. They were embedded in paraffin, and serial 4 μm sections were stained with H&E and Masson's trichrome stain. The dermal thickness was calculated as the mean distance (the dermal-epidermal junction to the dermal-subcutaneous fat junction) from three randomly selected fields per specimen.

QUANTIFICATION AND STATISTICAL ANALYSIS

Data were analyzed and represented graphically using GraphPad Prism v8 software. Mean ± standard error of the mean (SEM) of at least three independent experiments were calculated for all experiments. The unpaired two-tailed Student's *t*-test was used for comparison of means between two independent groups; and the one-way ANOVA was used for comparison of means between two or more groups. If the *p*-value was less than 0.05, the differences were considered statistically significant. For statistical details of specific experiments, please see the respective figure legends.

Supplementary Material

Refer to Web version on PubMed Central for supplementary material.

ACKNOWLEDGMENTS

This research was supported by the Intramural Research Programs of NIDCR, NHBLI, and NCI, National Institutes of Health (NIH), United States of America, and The National Key R&D Programme of China (2020YFA0710800 to L.S.), China. We would like to thank the Combined Technical Research Core (ZIC DE000729–09) and Veterinary Resources Core (ZICDE000740–05) at NIDCR for service and technical assistance.

REFERENCES

1. Papadimitriou TI, van Caam A, van der Kraan PM, and Thurlings RM (2022). Therapeutic Options for Systemic Sclerosis: Current and Future Perspectives in Tackling Immune-Mediated Fibrosis. Biomedicines 10, 316. 10.3390/biomedicines10020316. [PubMed: 35203525]
2. Fuschiotti P (2016). Current perspectives on the immunopathogenesis of systemic sclerosis. ImmunoTargets Ther. 5, 21–35. 10.2147/ITT.S82037. [PubMed: 27529059]
3. Dardalhon V, Collins M, and Kuchroo VK (2015). Physical attraction of Th9 cells is skin deep. Ann. Transl. Med. 3, 74. 10.3978/j.issn.2305-5839.2015.01.28. [PubMed: 25992373]
4. Nakatsukasa H, Zhang D, Maruyama T, Chen H, Cui K, Ishikawa M, Deng L, Zanvit P, Tu E, Jin W, et al. (2015). The DNA-binding inhibitor Id3 regulates IL-9 production in CD4(+) T cells. Nat. Immunol. 16, 1077–1084. 10.1038/ni.3252. [PubMed: 26322481]
5. Park SA, Lim YJ, Ku WL, Zhang D, Cui K, Tang LY, Chia C, Zanvit P, Chen Z, Jin W, et al. (2022). Opposing functions of circadian protein DBP and atypical E2F family E2F8 in anti-tumor Th9 cell differentiation. Nat. Commun. 13, 6069. 10.1038/s41467-022-33733-8. [PubMed: 36241625]
6. Zhang YE (2017). Non-Smad Signaling Pathways of the TGF-beta Family. Cold Spring Harbor Perspect. Biol. 9, a022129. 10.1101/cshperspect.a022129.
7. Sorrentino A, Thakur N, Grimsby S, Marcusson A, von Bulow V, Schuster N, Zhang S, Heldin CH, and Landström M (2008). The type I TGF-beta receptor engages TRAF6 to activate TAK1 in a receptor kinase-independent manner. Nat. Cell Biol. 10, 1199–1207. 10.1038/ncb1780. [PubMed: 18758450]
8. Xiao X, Balasubramanian S, Liu W, Chu X, Wang H, Taparowsky EJ, Fu YX, Choi Y, Walsh MC, and Li XC (2012). OX40 signaling favors the induction of T(H)9 cells and airway inflammation. Nat. Immunol. 13, 981–990. 10.1038/ni.2390. [PubMed: 22842344]
9. Abdelaziz MH, Wang H, Cheng J, and Xu H (2020). Th2 cells as an intermediate for the differentiation of naive T cells into Th9 cells, associated with the Smad3/Smad4 and IRF4 pathway. Exp. Ther. Med. 19, 1947–1954. 10.3892/etm.2020.8420. [PubMed: 32104253]
10. Elyaman W, Bassil R, Bradshaw EM, Orent W, Lahoud Y, Zhu B, Radtke F, Yagita H, and Khoury SJ (2012). Notch receptors and Smad3 signaling cooperate in the induction of interleukin-9-producing T cells. Immunity 36, 623–634. 10.1016/j.immuni.2012.01.020. [PubMed: 22503540]
11. Bartel DP (2004). MicroRNAs: genomics, biogenesis, mechanism, and function. Cell 116, 281–297. 10.1016/s0092-8674(04)00045-5. [PubMed: 14744438]
12. Ho PTB, Clark IM, and Le LTT (2022). MicroRNA-Based Diagnosis and Therapy. Int. J. Mol. Sci. 23, 7167. 10.3390/ijms23137167. [PubMed: 35806173]
13. Rodriguez-Galan A, Fernandez-Messina L, and Sanchez-Madrid F (2018). Control of Immunoregulatory Molecules by miRNAs in T Cell Activation. Front. Immunol. 9, 2148. 10.3389/fimmu.2018.02148. [PubMed: 30319616]
14. Dosil SG, Rodriguez-Galan A, Sanchez-Madrid F, and Fernandez-Messina L (2022). MicroRNAs in T Cell-Immunotherapy. Int. J. Mol. Sci. 24, 250. 10.3390/ijms24010250. [PubMed: 36613706]
15. Naqvi RA, Datta M, Khan SH, and Naqvi AR (2022). Regulatory roles of MicroRNA in shaping T cell function, differentiation and polarization. Semin. Cell Dev. Biol. 124, 34–47. 10.1016/j.semcdb.2021.08.003. [PubMed: 34446356]
16. Jiang S, Li C, Olive V, Lykken E, Feng F, Sevilla J, Wan Y, He L, and Li QJ (2011). Molecular dissection of the miR-17–92 cluster's critical dual roles in promoting Th1 responses and preventing inducible Treg differentiation. Blood 118, 5487–5497. 10.1182/blood-2011-05-355644. [PubMed: 21972292]
17. Simpson LJ, Patel S, Bhakta NR, Choy DF, Brightbill HD, Ren X, Wang Y, Pua HH, Baumjohann D, Montoya MM, et al. (2014). A microRNA upregulated in asthma airway T cells promotes TH2 cytokine production. Nat. Immunol. 15, 1162–1170. 10.1038/ni.3026. [PubMed: 25362490]
18. Liu SQ, Jiang S, Li C, Zhang B, and Li QJ (2014). miR-17–92 cluster targets phosphatase and tensin homology and Ikaros Family Zinc Finger 4 to promote TH17-mediated inflammation. J. Biol. Chem. 289, 12446–12456. 10.1074/jbc.M114.550723. [PubMed: 24644282]

19. Yamashita M, Fatyol K, Jin C, Wang X, Liu Z, and Zhang YE (2008). TRAF6 mediates Smad-independent activation of JNK and p38 by TGF-beta. Mol. Cell 31, 918–924. 10.1016/j.molcel.2008.09.002. [PubMed: 18922473]
20. Laine A, and Ronai Z (2005). Ubiquitin chains in the ladder of MAPK signaling. Sci. STKE 2005, re5. 10.1126/stke.2812005re5. [PubMed: 15855411]
21. Walsh MC, Lee J, and Choi Y (2015). Tumor necrosis factor receptor-associated factor 6 (TRAF6) regulation of development, function, and homeostasis of the immune system. Immunol. Rev. 266, 72–92. 10.1111/imr.12302. [PubMed: 26085208]
22. Sun D, Xu J, Zhang W, Song C, Gao C, He Y, and Shang Y (2022). Negative regulator NLRC3: Its potential role and regulatory mechanism in immune response and immune-related diseases. Front. Immunol. 13, 1012459. 10.3389/fimmu.2022.1012459. [PubMed: 36341336]
23. Zhou L, Ma Q, Shi H, and Huo K (2010). NUMBL interacts with TRAF6 and promotes the degradation of TRAF6. Biochem. Biophys. Res. Commun. 392, 409–414. 10.1016/j.bbrc.2010.01.037. [PubMed: 20079715]
24. Swarnkar G, Chen THP, Arra M, Nasir AM, Mbalaviele G, and Abu-Amer Y (2017). NUMBL Interacts with TAK1, TRAF6 and NEMO to Negatively Regulate NF-kappaB Signaling During Osteoclastogenesis. Sci. Rep. 7, 12600. 10.1038/s41598-017-12707-7. [PubMed: 28974699]
25. Li J, Liu N, Tang L, Yan B, Chen X, Zhang J, and Peng C (2020). The relationship between TRAF6 and tumors. Cancer Cell Int. 20, 429. 10.1186/s12935-020-01517-z. [PubMed: 32905356]
26. Lu Y, Wang Q, Xue G, Bi E, Ma X, Wang A, Qian J, Dong C, and Yi Q (2018). Th9 Cells Represent a Unique Subset of CD4(+) T Cells Endowed with the Ability to Eradicate Advanced Tumors. Cancer Cell 33, 1048–1060.e7. 10.1016/j.ccell.2018.05.004. [PubMed: 29894691]
27. Oh H, and Ghosh S (2013). NF-kappaB: roles and regulation in different CD4(+) T-cell subsets. Immunol. Rev. 252, 41–51. 10.1111/imr.12033. [PubMed: 23405894]
28. Chen T, Guo J, Cai Z, Li B, Sun L, Shen Y, Wang S, Wang Z, Wang Z, Wang Y, et al. (2020). Th9 Cell Differentiation and Its Dual Effects in Tumor Development. Front. Immunol. 11, 1026. 10.3389/fimmu.2020.01026. [PubMed: 32508847]
29. Guggino G, Lo Pizzo M, Di Liberto D, Rizzo A, Cipriani P, Ruscitti P, Candore G, Gambino CM, Sireci G, Dieli F, et al. (2017). Interleukin-9 over-expression and T helper 9 polarization in systemic sclerosis patients. Clin. Exp. Immunol. 190, 208–216. 10.1111/cei.13009. [PubMed: 28681919]
30. Bobeica C, Niculet E, Musat CL, Craescu M, Stefanescu BI, Dinu C, Chiscop I, Chirobocea S, Nechita L, Iancu AV, et al. (2022). Paraclinical Aspects in Systemic Sclerosis. Int. J. Gen. Med. 15, 4391–4398. 10.2147/IJGM.S355662. [PubMed: 35502184]
31. Chen C, Akiyama K, Wang D, Xu X, Li B, Moshaverinia A, Brombacher F, Sun L, and Shi S (2015). mTOR inhibition rescues osteopenia in mice with systemic sclerosis. J. Exp. Med. 212, 73–91. 10.1084/jem.20140643. [PubMed: 25534817]
32. Goswami R, and Kaplan MH (2012). Yoking OX40 to regulation of IL-9. Nat. Immunol. 13, 942–943. 10.1038/ni.2421. [PubMed: 22990899]
33. Giunti D, Marini C, Parodi B, Usai C, Milanese M, Bonanno G, Kerlero de Rosbo N, and Uccelli A (2021). Role of miRNAs shuttled by mesenchymal stem cell-derived small extracellular vesicles in modulating neuroinflammation. Sci. Rep. 11, 1740. 10.1038/s41598-021-81039-4. [PubMed: 33462263]
34. Kuo G, Wu CY, and Yang HY (2019). MiR-17–92 cluster and immunity. J. Formos. Med. Assoc. 118, 2–6. 10.1016/j.jfma.2018.04.013. [PubMed: 29857952]
35. Li ZL, Li D, and Yin GQ (2022). MiR-19b-3p promotes tumor progression of non-small cell lung cancer via downregulating HOXA9 and predicts poor prognosis in patients. Histol. Histopathol. 37, 779–789. 10.14670/HH-18-448. [PubMed: 35274735]
36. Zhang Y, Lu W, Chen Y, Lin Y, Yang X, Wang H, and Liu Z (2021). The miR-19b-3p-MAP2K3-STAT3 feedback loop regulates cell proliferation and invasion in esophageal squamous cell carcinoma. Mol. Oncol. 15, 1566–1583. 10.1002/1878-0261.12934. [PubMed: 33660414]
37. Hu X, Liu H, and Li C (2023). MiRNA-19b-3p downregulates the endothelin B receptor in gastric cancer cells to prevent angiogenesis and proliferation. Acta Biochim. Pol. 70, 363–370. 10.18388/abp.2020_6595. [PubMed: 37226719]

38. Nazarov PV, Reinsbach SE, Muller A, Nicot N, Philippidou D, Vallar L, and Kreis S (2013). Interplay of microRNAs, transcription factors and target genes: linking dynamic expression changes to function. Nucleic Acids Res. 41, 2817–2831. 10.1093/nar/gks1471. [PubMed: 23335783]

39. Xu H, Zhang J, Shi X, Li X, and Zheng C (2021). NF-kappaB inducible miR-30b-5p aggravates joint pain and loss of articular cartilage via targeting SIRT1-FoxO3a-mediated NLRP3 inflammasome. Aging (Albany NY) 13, 20774–20792. 10.18632/aging.203466. [PubMed: 34455406]

40. Zhao Y, Bhattacharjee S, Jones BM, Hill J, Dua P, and Lukiw WJ (2014). Regulation of neurotropic signaling by the inducible, NF-kB-sensitive miRNA-125b in Alzheimer's disease (AD) and in primary human neuronal-glial (HNG) cells. Mol. Neurobiol. 50, 97–106. 10.1007/s12035-013-8595-3. [PubMed: 24293102]

41. Taganov KD, Boldin MP, Chang KJ, and Baltimore D (2006). NF-kappaB-dependent induction of microRNA miR-146, an inhibitor targeted to signaling proteins of innate immune responses. Proc. Natl. Acad. Sci. USA 103, 12481–12486. 10.1073/pnas.0605298103. [PubMed: 16885212]

42. Alexandrov P, Zhai Y, Li W, and Lukiw W (2019). Lipopolysaccharide-stimulated, NF-kB-miRNA-146a- and miRNA-155-mediated molecular-genetic communication between the human gastrointestinal tract microbiome and the brain. Folia Neuropathol. 57, 211–219. 10.5114/fn.2019.88449. [PubMed: 31588707]

43. Imaizumi T, Tanaka H, Tajima A, Yokono Y, Matsumiya T, Yoshida H, Tsuruga K, Aizawa-Yashiro T, Hayakari R, Inoue I, et al. (2010). IFN-gamma and TNF-alpha synergistically induce microRNA-155 which regulates TAB2/IP-10 expression in human mesangial cells. Am. J. Nephrol. 32, 462–468. 10.1159/000321365. [PubMed: 20948191]

44. Ciccia F, Guggino G, Ferrante A, Cipriani P, Giacomelli R, and Triolo G (2016). Interleukin-9 and T helper type 9 cells in rheumatic diseases. Clin. Exp. Immunol. 185, 125–132. 10.1111/cei.12807. [PubMed: 27159882]

45. van den Hoogen F, Khanna D, Fransen J, Johnson SR, Baron M, Tyndall A, Matucci-Cerinic M, Naden RP, Medsger TA Jr., Carreira PE, et al. (2013). 2013 classification criteria for systemic sclerosis: an American College of Rheumatology/European League against Rheumatism collaborative initiative. Arthritis Rheum. 65, 2737–2747. 10.1002/art.38098. [PubMed: 24122180]

46. Khanna D, Furst DE, Clements PJ, Allanore Y, Baron M, Czirjak L, Distler O, Foeldvari I, Kuwana M, Matucci-Cerinic M, et al. (2017). Standardization of the modified Rodnan skin score for use in clinical trials of systemic sclerosis. J. Scleroderma Relat. Disord. 2, 11–18. 10.5301/jsrd.5000231. [PubMed: 28516167]

Highlights

- TGF-β and IL-4 induce *miR-19b* in $CD4^+$ T cells by TRAF6-TAK1-NF-κB p65 axis
- *miR-19b* promotes *Il9* gene expression by suppressing E2f8 in Th9 cells
- *miR-19b*-induced IL-9 is crucial for SSc pathogenesis
- In patients with SSc, increased *IL9* and *MIR-19B* exacerbate the disease progression

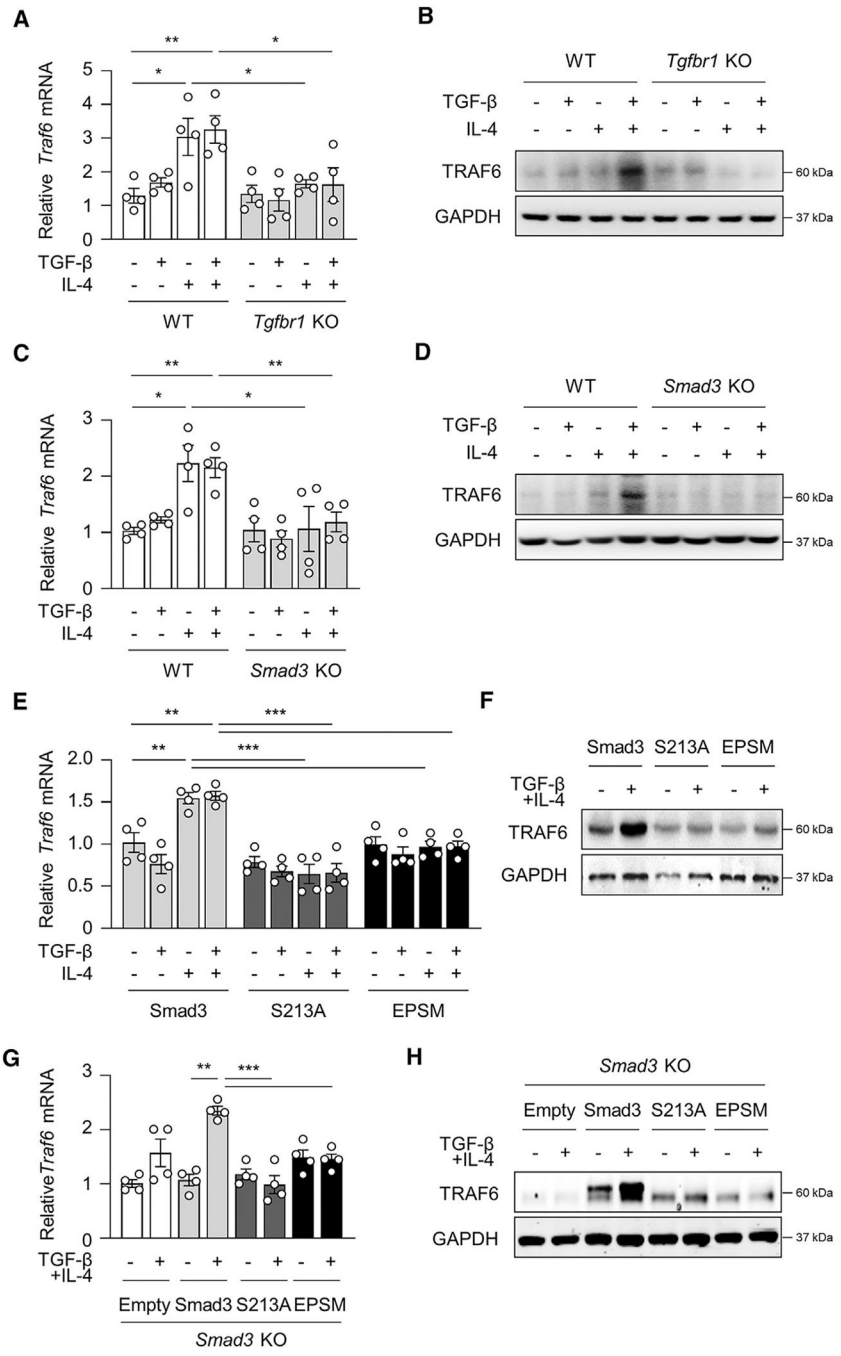

Figure 1. TRAF6 is increased by activation of Smad3-Ser^{213} during Th9 differentiation induced by IL-4 plus TGF-β

(A and B) Expression of *Traf6* mRNA by real-time PCR (A) and TRAF6 protein by western immunoblotting (B) in CD4^{+} T cells from *Tgfbr1*$^{f/f}$-ER^{Cre-} (WT) and *Tgfbr1*$^{f/f}$-ER^{Cre+} (*Tgfbr1* KO) mice in response to TGF-β, IL-4, or TGF-β plus IL-4 for 2 h.

(C and D) Expression of *Traf6* mRNA by real-time PCR (C) and TRAF6 protein by western immunoblotting (D) in CD4^{+} T cells from *Smad3* WT and *Smad3* KO mice in response to TGF-β, IL-4, or TGF-β plus IL-4 for 2 h.

(E–H) Real-time PCR (E and G) and immunoblotting of TRAF6 expression (F and H) in normal T cells and S213A mutant- or EPSM mutant-transfected WT $CD4^+$ T cells (E and F) or *Smad3* KO T cells (G and H) cultured with IL-4 and TGF-β for 2 h.

For (A), (C), (E), and (G), data are from four independent experiments. For (B), (D), (F), and (H), data are pooled from three experiments. Data were analyzed by two-way ANOVA with Tukey's test. Graphs show the mean ± SEM.

See also Figure S1.

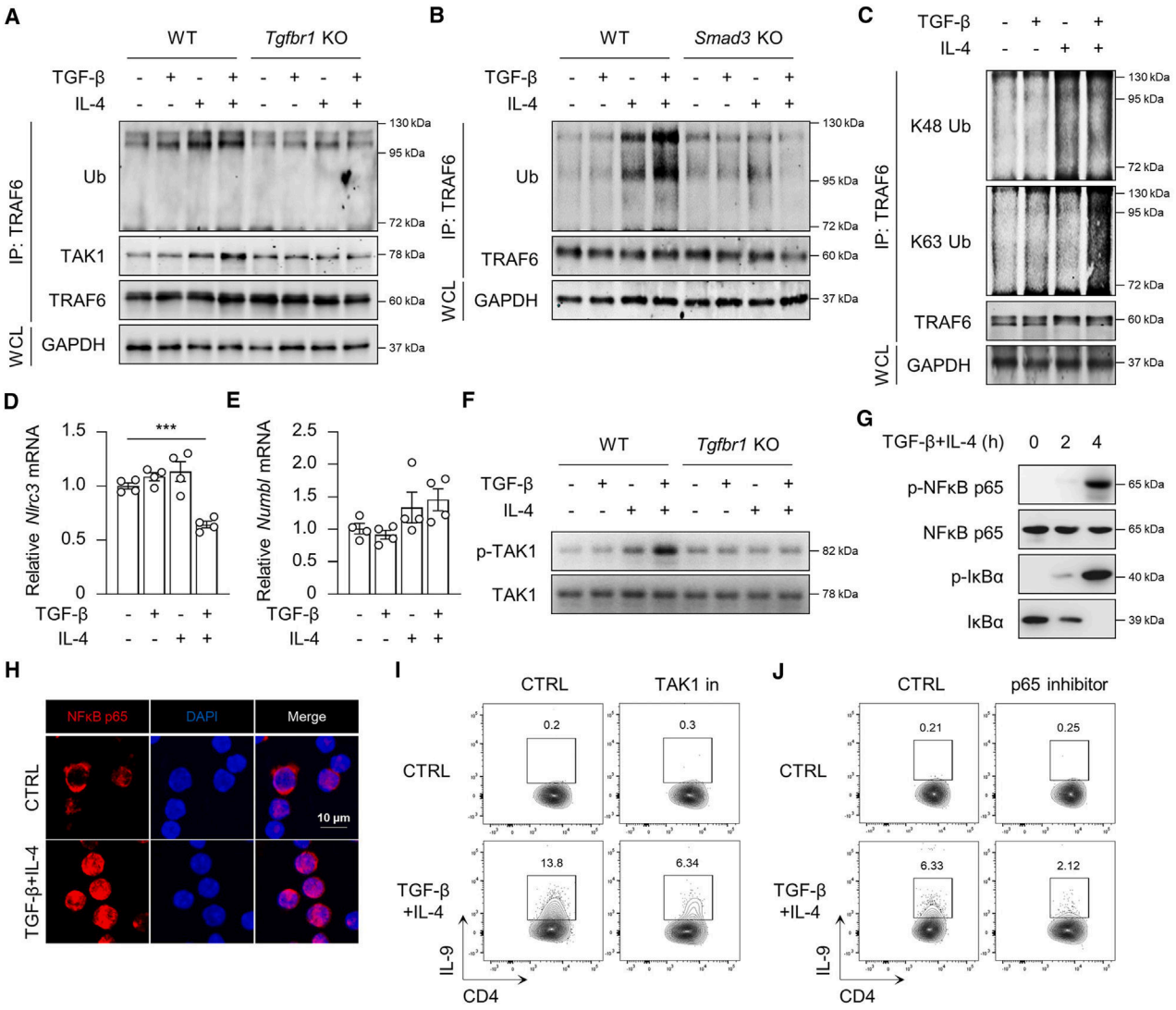

Figure 2. K63 ubiquitination of TRAF6 enhances TAK1 and NF-κB activation during Th9 differentiation

(A) Immunoprecipitation (IP) of TRAF6 in CD4$^+$ T cells from WT and *Tgfbr1* KO mice incubated with TGF-β, IL-4, or TGF-β plus IL-4 for 2 h, followed by immunoblot analysis with anti-ubiquitin (Ub), anti-TRAF6, and anti-TAK1. Whole-cell lysates (WCLs) were used for immunoblotting with anti-GAPDH.

(B) IP of TRAF6 in CD4$^+$ T cells from *Smad3* WT and *Smad3* KO mice incubated with TGF-β, IL-4, or TGF-β plus IL-4 for 2 h, followed by immunoblot analysis with anti-Ub and anti-TRAF6.

(C) IP of TRAF6 in naive CD4$^+$ T cells and analysis using immunoblotting with anti-Ub-K48- or anti-Ub-K63-specific antibody.

(D and E) Expression of *Nlrc3* and *Numbl* mRNA in CD4$^+$ T cells cultured with TGF-β, IL-4, or TGF-β plus IL-4 for 1 h.

(F) Immunoblotting of TAK1 in WT and *Tgfbr1* KO T cells after 4 h stimulation.

(G) Immunoblotting of NF-κB p65 and IκB in TGF-β-and-IL-4-treated T cells for the indicated time periods.

(H) Immunofluorescence microscopy analysis of NF-κB p65 nuclear translocation in T cells cultured with TGF-β and IL-4 for 4 h.

(I and J) Intracellular staining of IL-9 in $CD4^+$ T cells in the presence of TAK1inhibitor (I) or p65 inhibitor (J) and cultured with TGF-β plus IL-4 for 72 h.

For (A)–(C), (F), (G), and (H)–(J), data are pooled from three experiments. For (D) and (E), data are from four independent experiments. Data were analyzed by two-way ANOVA with Tukey's test. Graphs show the mean ± SEM.

See also Figure S2.

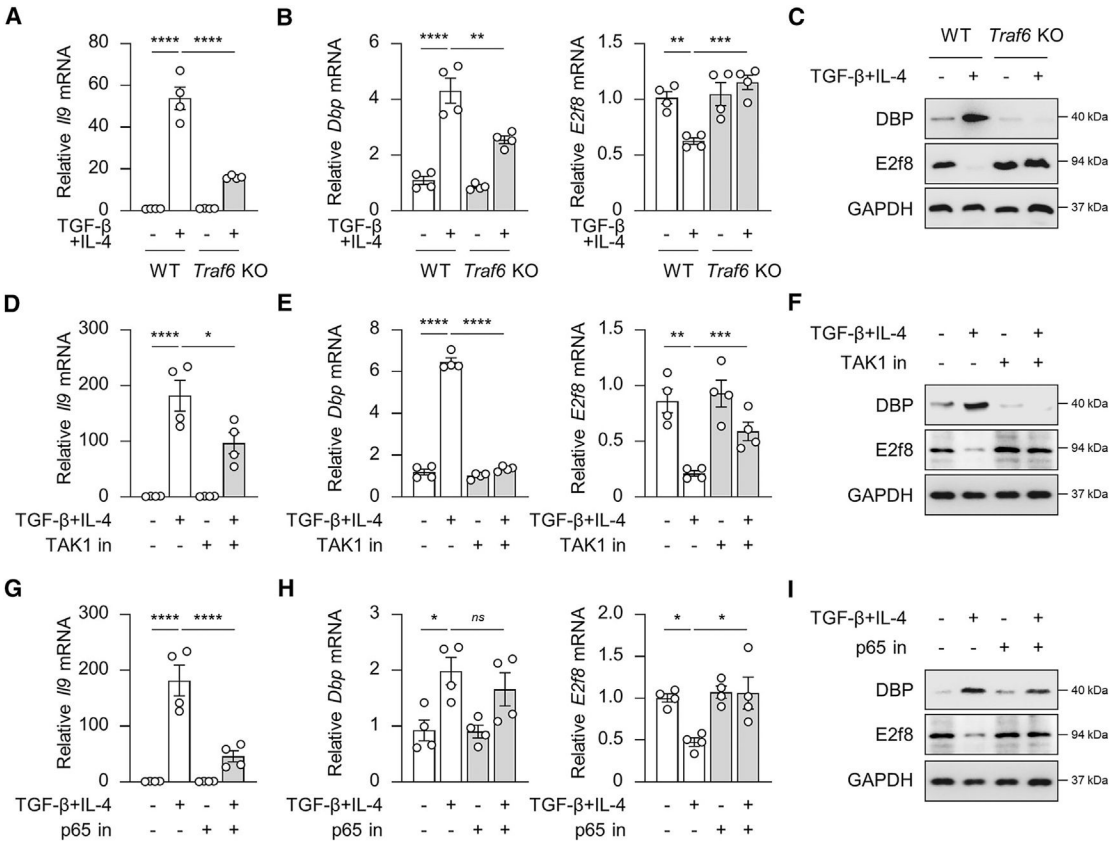

Figure 3. The TRAF6-TAK1-NF-κB axis is required for E2f8 downregulation to Th9 differentiation

(A–C) Expression of *Il9* mRNA (A) and *Dbp* and *E2f8* mRNA (B) after 24 h and immunoblotting of DBP and E2f8 protein (C) after 72 h in WT and *Traf6* KO T cells. (D–F) Expression of *Il9* mRNA (D) and *Dbp* and *E2f8* mRNA (E) after 24 h and immunoblotting of DBP and E2f8 protein (F) after 72 h in TAK1-inhibited T cells. (G–I) Expression of *Il9* mRNA (G) and *Dbp* and *E2f8* mRNA (H) after 24 h and immunoblotting of DBP and E2f8 protein (I) after 72 h in p65-inhibited T cells. For (A), (B), (D), (E), (G), and (H), data are from four independent experiments. For (C), (F), and (I), data are pooled from three experiments. Data were analyzed by two-way ANOVA with Tukey's test. Graphs show the mean ± SEM.

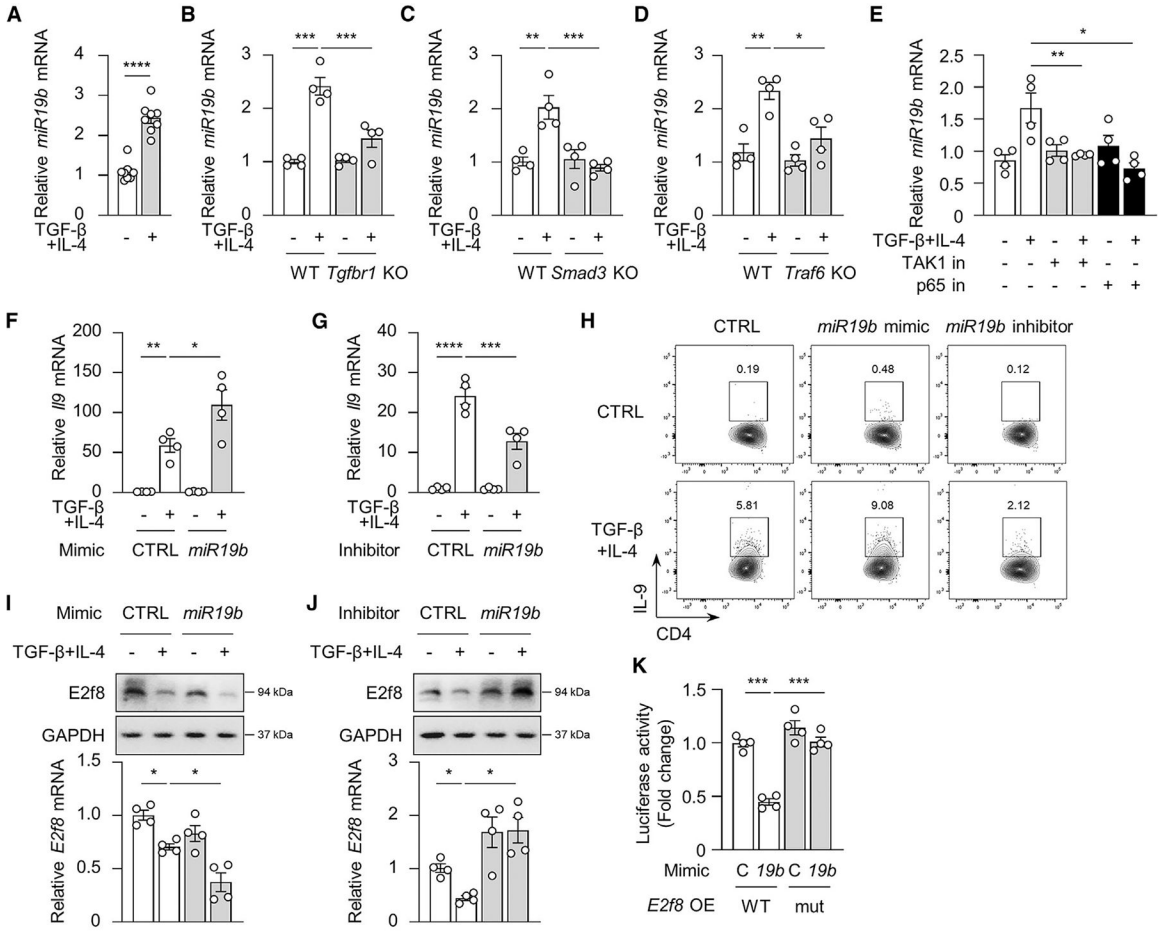

Figure 4. *miR-19b* leads to Th9 polarization via *E2f8* suppression

(A) Expression of *miR-19b* in CD4$^+$ T cells cultured with TGF-β plus IL-4 for 24 h.

(B–D) Expression of *miR-19b* in WT and *Tgfbr1* KO (B), *Smad3* KO (C), and *Traf6* KO (D) T cells in response to TGF-β plus IL-4 for 24 h.

(E) Expression of *miR-19b* in T cells treated with TGF-β plus IL-4 in the presence or absence of TAK1 inhibitor or p65 inhibitor.

(F–H) Expression of *Il9* mRNA (F and G) and intracellular IL-9 production (H) in negative control-, *miR-19b* mimic-, or *miR-19b* inhibitor-transfected CD4$^+$ T cells, followed by the stimulation of TGF-β and IL-4 for 72 h.

(I and J) Expression of *E2f8* mRNA and E2f8 protein in *miR-19b*-overexpressed cells in (F) or *miR-19b* inhibited T cells in (G).

(K) Relative luciferase activity in HEK293 T cells overexpressing *miR-19b* and transfected with *E2f8* 3′ UTR WT or mutation vector (WT, *E2f8* WT; mut, *E2f8* point mutation in *miR-19b* binding site).

For (A)–(G) and (K), data are from four independent experiments. For (I) and (J), qPCR data are from four independent experiments, and western blots are pooled from three experiments. For (H), data are pooled from three experiments. Data were analyzed by two-way ANOVA with Tukey's test. Graphs show the mean ± SEM.

See also Figure S3.

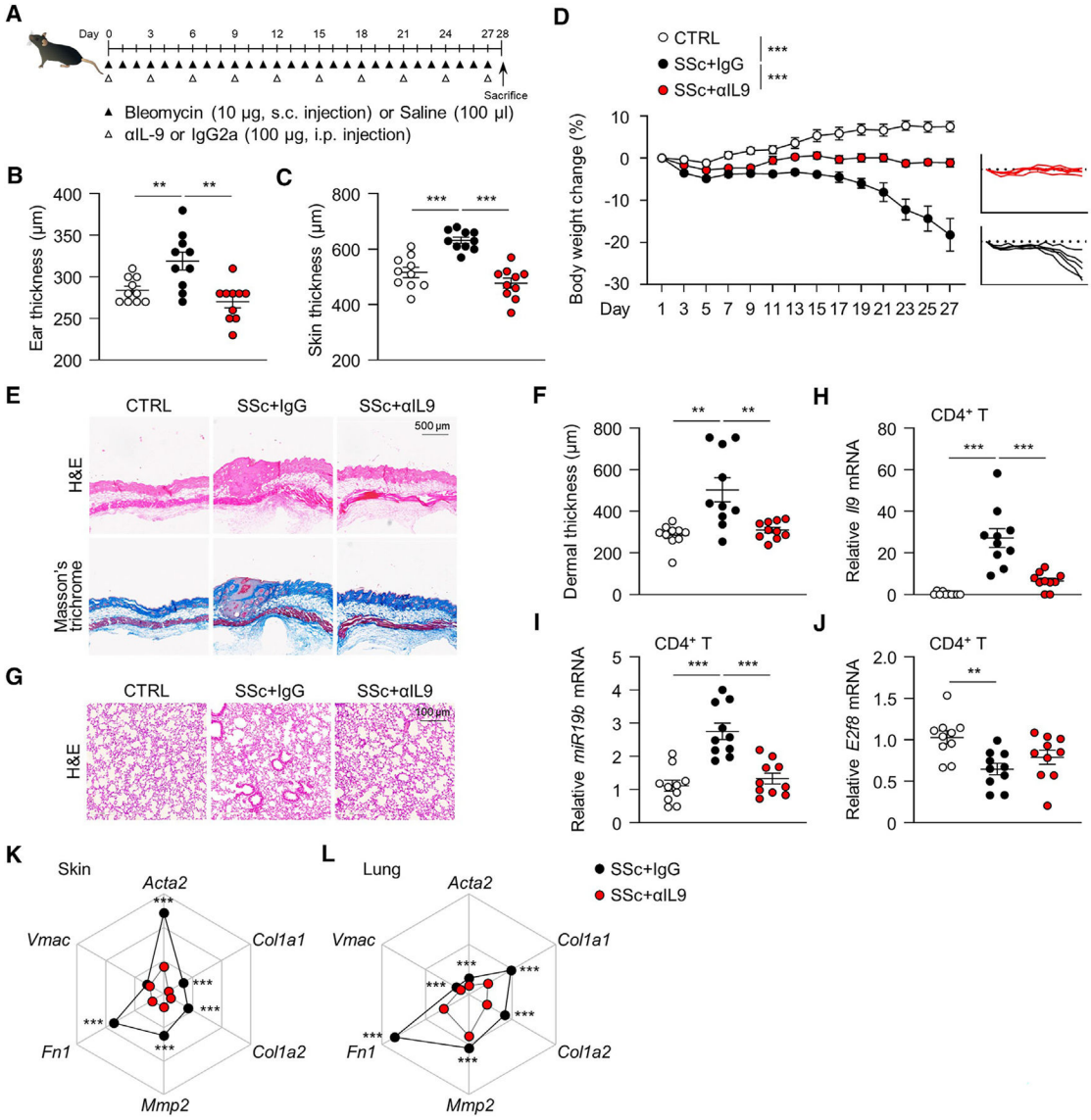

Figure 5. IL-9 blockade suppresses fibrogenic pathology in SSc mouse model *in vivo*

(A) Operational schematics of *in vivo* experiments. Mice were injected with bleomycin (BLM) subcutaneously (1 mg/kg/day) or saline (CTRL) for 28 days. For IL-9 neutralization, mice were treated intraperitoneally with anti-IL-9 antibody (100 μg) or mouse anti-IgG2a isotype control every 3 days.

(B–D) Skin thickness (B and C) and body weight (D) of CTRL and BLM-induced SSc mice injected with isotype control or anti-IL-9 antibody.

(E) H&E staining and Masson's trichrome staining of the skin tissues from CTRL-, BLM-plus-IgG-, and BLM-plus-anti-IL-9-treated mice at 28 days.

(F) The thickness of the dermal layer in (E).

(G) H&E staining of the lung tissues in the same treatments as in (E).

(H–J) Expression of *Il9*, *miR-19b*, and *E2f8* in $CD4^+$ T cells isolated from spleens and lymph nodes.

(K and L) Spider plots of fibrogenic genes including *Acta2, Col1a1, Col1a2, Mmp2, Fn1*, and *Vmac* in skin (K) and lung (L).

These data are representative of two independent experiments, $n = 10$ per group. Data were analyzed by two-tailed unpaired Student's t test. Graphs show the mean ± SEM.

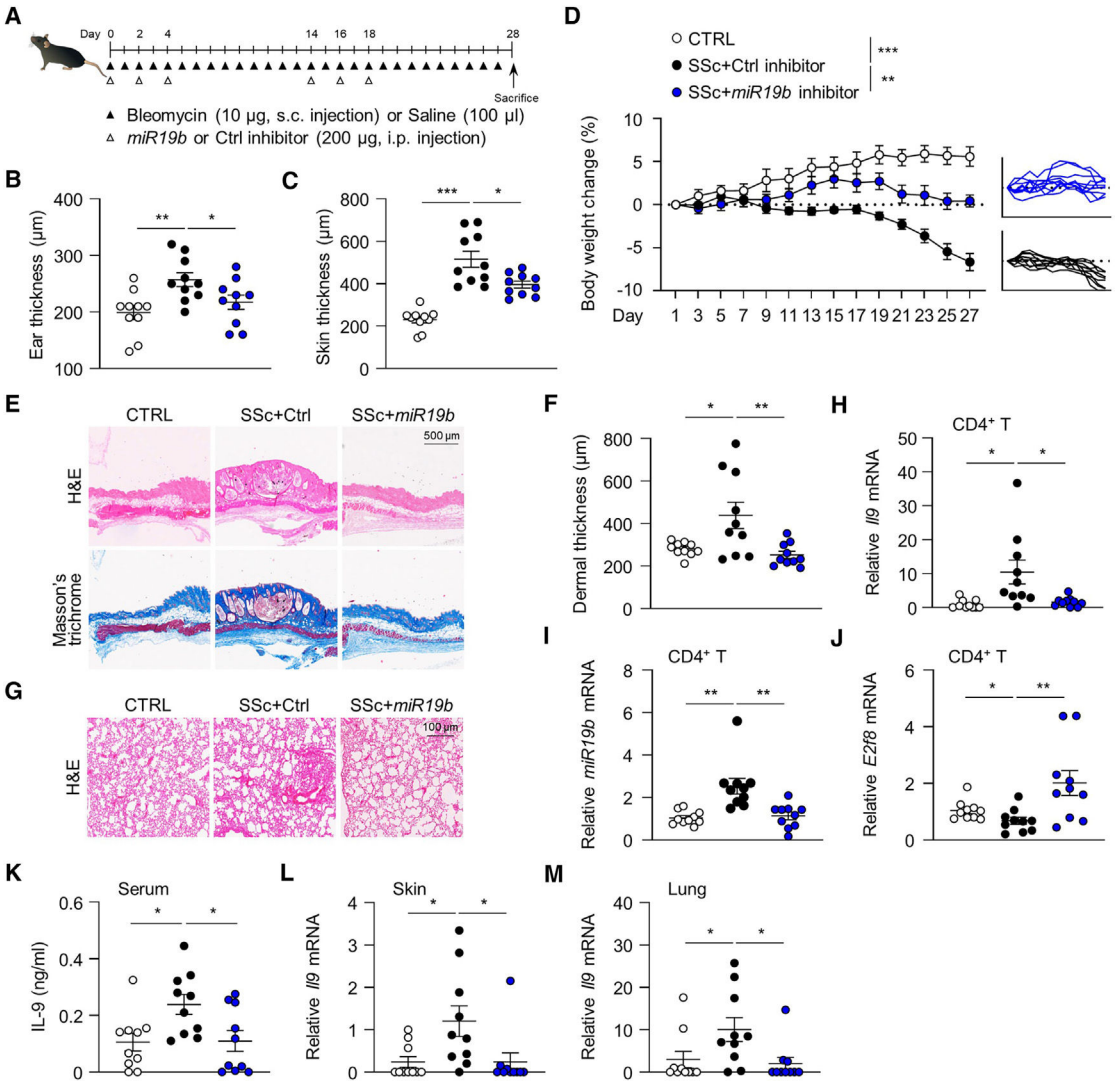

Figure 6. *miR-19b* blockade inhibits BLM-induced fibrosis by IL-9 suppression *in vivo*

(A) Operational schematics of *in vivo* experiments. Mice were injected with BLM or saline (CTRL) in the same treatments as in Figure 5A and then treated with MiRCURY LNA *miR-19b* inhibitor (200 μg) or control inhibitor on days 1, 3, 5, 15, 17, and 19 (6 times).

(B–D) Skin thickness (B and C) and body weight (D) of CTRL and BLM-induced SSc mice injected with control (Ctrl) inhibitor or *miR-19b* inhibitor.

(E) H&E staining and Masson's trichrome staining of the skin tissues from CTRL-, BLM-plus-Ctrl-inhibitor-, and BLM-plus-*miR-19b*-inhibitor-treated mice at 28 days.

(F) The thickness of the dermal layer in (E).

(G) H&E staining of the lung tissues in the same treatments as in (E).

(H–J) Expression of *Il9*, *miR-19b*, and *E2f8* in $CD4^+$ T cells isolated from spleens and lymph nodes.

(K) IL-9 production by ELISA assay in blood serum.

(L and M) Expression of *Il9* in skin and lung.

These data are representative of two independent experiments, $n = 10$ per group. Data were analyzed by two-tailed unpaired Student's t test. Graphs show the mean ± SEM.
See also Figures S4 and S5.

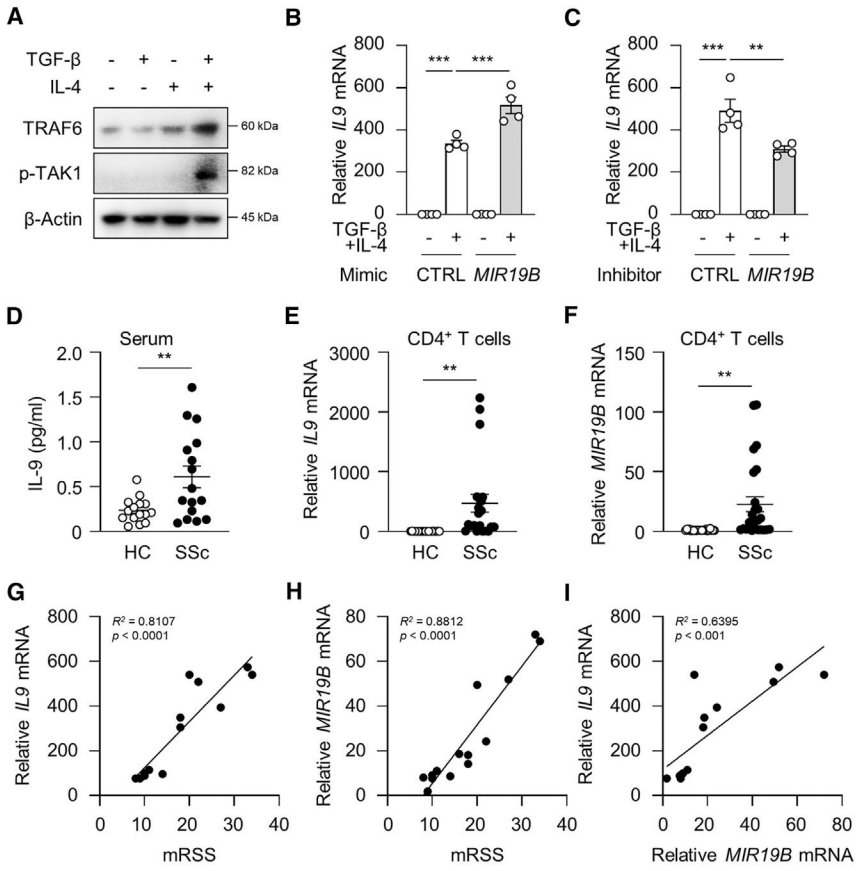

Figure 7. *miR-19b* expression in T cells of the patients with SSc

(A) Immunoblotting of TRAF6 and p-TAK-1 in human naive $CD4^+$ T cells cultured with IL-4 and TGF-β for 4 h.

(B and C) Expression of *IL9* mRNA in negative control-, *MIR-19B* mimic- or *MIR-19B* inhibitor-transfected human $CD4^+$ T cells, followed by the stimulation of TGF-β and IL-4 for 72 h.

(D) Expression of IL-9 protein in blood serum from patients with SSc ($n = 16$) and healthy controls ($n = 15$).

(E and F) Expression of *IL9* and *MIR-19B* mRNA in $CD4^+$ T cells isolated from blood of the patients ($n = 26$) and healthy individuals ($n = 22$).

(G and H) Correlation of *IL9* and *MIR-19B* mRNA with the mRSS of the patients ($n = 14$): *IL9* ($R^2 = 0.8107$, $p < 0.0001$) and *MIR-19B* ($R^2 = 0.8812$, $p < 0.0001$).

(I) Scatterplot of *MIR-19B* on the x axis and *IL9* on they axis in $CD4^+$ T cells from the patients ($n = 13$): ($R^2 = 0.6395$, $p < 0.001$).

Data were analyzed by two-tailed unpaired Student's t test. Graphs show the mean ± SEM. See also Figure S6 and Table S1.

KEY RESOURCES TABLE

REAGENT or RESOURCE	SOURCE	IDENTIFIER
Antibodies		
Purified anti-mouse CD3 (145-2C11)	Bio X Cell	Cat# BE0001-1; RRID: B_1107634
Purified anti-mouse CD28 (37.51)	Bio X Cell	Cat# BE0015-1; RRID: B_1107624
Purified anti-human CD3 (OKT-3)	Bio X Cell	Cat# BE0001-2; RRID: AB_1107632
Purified anti-human CD28 (9.3)	Bio X Cell	Cat# BE0248; RRID: AB_2687729
Anti-mouse IL-9 (9C1)	Bio X Cell	Cat# BE0181; RRID: AB_10950648
Mouse IgG2a Isotype Control (C1.18.4)	Bio X Cell	Cat# BE0085; RRID: AB_1107771
Anti-mouse CD3 PerCP/Cyanine5.5 (17A2)	BioLegend	Cat# 100218; RRID: AB_1595492
Anti-mouse CD4 Brilliant Violet 510 (RM4-5)	BioLegend	Cat# 100559; RRID: AB_2562608
Anti-mouse CD8a eFluor 450 (53-6.7)	Thermo Fisher Scientific	Cat# 48-0081-82; RRID: AB_1272198
Anti-mouse CD45 Alexa Fluor 700 (30-F11)	Thermo Fisher Scientific	Cat# 56-0451-82; RRID: AB_891454
Anti-mouse IL-4 Alexa Fluor 488 (11B11)	Thermo Fisher Scientific	Cat# 53-7041-82; RRID: AB_469922
Anti-mouse IL-9 PE (RM9A4)	BioLegend	Cat# 514103; RRID: AB_2126639
Anti-mouse IL-9 eFluor 660 (RM9A4)	Thermo Fisher Scientific	Cat# 50-8091-82; RRID: AB_11218680
Anti-mouse IL-10 FITC (JES5-16E3)	Thermo Fisher Scientific	Cat# 11-7101-82; RRID: AB_465403
Anti-mouse IL-13 PE (eBio13A)	Thermo Fisher Scientific	Cat# 12-7133-82; RRID: AB_763559
Anti-mouse IL-17A APC (eBio17B7)	Thermo Fisher Scientific	Cat# 17-7177-81; RRID: AB_763580
Anti-mouse IFN gamma APC (XMG1.2)	BioLegend	Cat# 505810; RRID: AB_315404
Anti-mouse FOXP3 PE-Cyanine7 (FJK-16 s)	Thermo Fisher Scientific	Cat# 25-5773-82; RRID: AB_891552
Anti-mouse CD140a PerCP/Cyanine5.5 (PDGFRA)	BioLegend	Cat# 135914; RRID: AB_2715986
Anti-human CD4 PerCP/Cyanine5.5 (OKT4)	Thermo Fisher Scientific	Cat# 45-0048-42; RRID: AB_10804390
Anti-human CD45 Alexa Fluor 700 (H130)	BioLegend	Cat# 304023; RRID: AB_493760
Anti-human CD44 APC (IM7)	Thermo Fisher Scientific	Cat# 17-0441-83; RRID: AB_469391
Anti-human IL-9 PE (MH9D1)	Thermo Fisher Scientific	Cat# 12-7098-42; RRID: AB_11151145
Anti-TRAF6 (D-10) Mouse	Santa Cruz Biotechnology	Cat#: sc-8409; RRID: AB_628391
Anti-Ub (FL-76) Rabbit	Santa Cruz Biotechnology	Cat# sc-9133; RRID: AB_2180553
Anti-K63-linkage Specific Polyubiquitin (D7A11) Rabbit	Cell Signaling Technology	Cat# 5621; RRID: AB_10827985
Anti-K48-linkage Specific Polyubiquitin (D9D5) Rabbit	Cell Signaling Technology	Cat# 8081; RRID: AB_10859893
Anti-phospho (Ser412)-TAK1 (MAP3K7) Rabbit	Cell Signaling Technology	Cat# 9339; RRID: AB_2140096
Anti-TAK1 (D94D7) Rabbit	Cell Signaling Technology	Cat# 5206; RRID: AB_10694079
Anti-phospho (Ser276)-NF-kappaB p65 Rabbit	Cell Signaling Technology	Cat# 3037; RRID: AB_2341216
Anti-NF-kappaB p65 (C22B4) Rabbit	Cell Signaling Technology	Cat# 4764; RRID: AB_823578
Anti-NLRC3 (Eowyn-1) Mouse	Novus	Cat# NBP2-80084; RRID: AB_3095882
Anti-DBP Rabbit	Abcam	Cat# ab22824; RRID: AB_447320
Anti-E2F8 Rabbit	Abcam	Cat# ab109596; RRID: AB_10887933
Anti-alpha-Smooth Muscle Actin (1A4) Mouse	Sigma-Aldrich	Cat# A2547; RRID: AB_476701
Anti-beta-Actin (13E5) Rabbit	Cell Signaling Technology	Cat# 4970; RRID: AB_2223172
Anti-GAPDH (D16H11) XP Rabbit	Cell Signaling Technology	Cat# 5174; RRID: AB_10622025
Anti-rabbit IgG, HRP-linked Ab	Cell Signaling Technology	Cat# 7074; RRID: AB_2099233

REAGENT or RESOURCE	SOURCE	IDENTIFIER
Anti-mouse IgG, HRP-linked Ab	Cell Signaling Technology	Cat# 7076; RRID: AB_330924
Goat anti-rabbit IgG, Alexa Fluor 594	Thermo Fisher Scientific	Cat# A-11012; RRID: AB_2534079
Goat anti-mouse IgG, Alexa Fluor 488	Thermo Fisher Scientific	Cat# A-11001; RRID: AB_2534069
Bacterial and virus strains		
pCL-ECO Packaging Vector	Addgene	Cat# 12371; RRID: Addgene_12371
pMSCV-IRES-GFP Empty Vector	Addgene	Cat# 21654; RRID: Addgene_21654
pmirGLO Dual-Luciferase miRNA Target Expression Vector	Promega	Cat# E1330
pLPCX-FLAG-*Smad3* Linker Mutations Retroviral Vector	Dr. Ying E. Zhang	N/A
Biological samples		
Mouse $CD4^+$ T cells	This paper	N/A
Mouse Pulmonary Fibroblasts	This paper	N/A
Human $CD4^+$ T cells, see Table S1	Collected from systemic sclerosis patients and healthy donors, NIH and Affiliated Drum Tower Hospital of Nanjing University Medical School	NIH (NCT000001846) and Drum Tower Hospital Ethics Committee (2008017)
Chemicals, peptides, and recombinant proteins		
Recombinant Human TGF-β1	R&D Systems	Cat# 240-B
Recombinant Mouse IL-4	R&D Systems	Cat# 404-ML
Recombinant Mouse IL-6	R&D Systems	Cat# 406-ML
Recombinant Mouse IL-9	R&D Systems	Cat# 409-ML
MEK/ERK Inhibitor (U0126)	Promega	Cat# V1121
JNK inhibitor II (SP600125)	Sigma-Aldrich	Cat# 420119
38 Inhibitor (SB203580)	Sigma-Aldrich	Cat# 559389
TAK1 Inhibitor (5z-7-Oxozeaenol)	Sigma-Aldrich	Cat# 499610
NFkB Activation Inhibitor II (JSH-23)	Millipore Sigma	Cat# 481408-M
Dulbecco's Modified Eagle Medium	Lonza	Cat# 12-733F
Fetal Bovine Serum	Gemini Bio-products	Cat# 100-106
L-Glutamine	Thermo Fisher Scientific	Cat# 25030081
MEM Non-Essential Amino Acids Solution	Thermo Fisher Scientific	Cat# 11140050
HEPES	Quality Biological	Cat# 118-089-721
β-Mercaptoethanol	Millipore Sigma	Cat# M3148
Sodium Pyruvate	Thermo Fisher Scientific	Cat# 11360070
Penicillin-Streptomycin	Thermo Fisher Scientific	Cat# 15140122
Polybrene Infection/Transfection Reagent	Millipore Sigma	Cat# TR-1003-G
TurboFect™ Transfection Reagent	Thermo Fisher Scientific	Cat# R0532
Lipofectamine™ RNAiMAX Transfection Reagent	Thermo Fisher Scientific	Cat# 13778150
DNase I	Millipore Sigma	Cat# DN25
Collagenase IV	Thermo Fisher Scientific	Cat# 17104-019

REAGENT or RESOURCE	SOURCE	IDENTIFIER
Dispase II	Roche	Cat# 04942078001
ACK Lysis Buffer	Qualty Biological	Cat# 118-156-101
Golgi-Plug Protein Transport Inhibitor	BD Biosciences	Cat# 555029
Percoll Density Gradient Media	Cytiva	Cat# 17089101
Ionomycin Calcium Salt	Millipore Sigma	Cat# I3909
PMA (phorbol 12-myristate 13-acetate)	Millipore Sigma	Cat# P8139
EDTA	Quality Biological	Cat# 351-027-101
Dimethyl Sulfoxide	Sigma-Aldrich	Cat# D2650
RIPA Lysis and Extraction Buffer	Thermo Fisher Scientific	Cat# 89900
Protease/Phosphatase Inhibitor Cocktail	Roche	Cat# 11836153001
Immobilon Western Chemiluminescent HRP Substrate	Millipore Sigma	Cat# WBKLS0050
Bleomycin Sulfate	Millipore Sigma	Cat# B1141000
Paraformaldehyde	Electron Microscopy Sciences	Cat# 15714-S
DAPI	Sigma-Aldrich	Cat# D9542-1MG
PBS, pH7.4	Gibco	Cat# 10010031
Critical commercial assays		
Naive $CD4^+$ T cell Isolation Kit, Mouse	Miltenyi Biotec	Cat# 130-104-453
Naive $CD4^+$ T cell Isolation Kit, Human	Miltenyi Biotec	Cat# 130-094-131
Cytofix/Cytoperm Fixation/Permeabilization Solution Kit	BD Biosciences	Cat# 554714
Foxp3/Transcription Factor Staining Buffer Set	Thermo Fisher Scientific	Cat# 00-5523-00
QuikChange Site-Directed Mutagenesis Kit	Agilent Technologies	Cat# 200523
Dynabeads™ Protein G Immunoprecipitation Kit	Thermo Fisher Scientific	Cat# 10007D
Dual-Luciferase Assay Systems Kit	Promega	Cat# E1500
Mouse IL-9 ELISA Kit	BioLegend	Cat# 442704
Human IL-9 ELISA Kit	BioLegend	Cat# 434704
RNeasy Mini Kit	Qiagen	Cat# 74104
miRNeasy Serum/Plasma Kit	Qiagen	Cat# 217184
cDNA Reverse Transcription Kit	Applied Biosystems	Cat# 4368814
TaqMan Gene Expression Master Mix	Applied Biosystems	Cat# 4369016
TagMan™ Advanced miRNA cDNA Synthesis Kit	Applied Biosystems	Cat# A28007
nCounter Mouse v1.5 miRNA Expression Assay Kit	NanoString Technologies	N/A
Deposited data		
MicroRNA Sequencing Data	This manuscript or NCBI Gene Expression Omnibus Database	GSE: 269954
Experimental models: Cell lines		
HEK293T cells	ATCC	Cat# ACS-4500; RRID: CVCL_4V93
Experimental models: Organisms/strains		

REAGENT or RESOURCE	SOURCE	IDENTIFIER
Mouse: C57BL/6	The Jackson Laboratory	Cat# 000664; RRID: IMSR_JAX:000664
Mouse: *Tgfbr1*$^{f/f}$	The Jackson Laboratory	Cat# 028701; RRID: IMSR_JAX:028701
Mouse: *Smad3* KO	The Jackson Laboratory	Cat# 003451; RRID: IMSR_JAX:003451
Mouse: *Traf6*$^{f/f}$	The Jackson Laboratory	Cat# 030849; RRID: IMSR_JAX:030849
Mouse: CD4-cre/ERT2	The Jackson Laboratory	Cat# 022356; RRID: IMSR_JAX:022356
Mouse: CD4-cre	The Jackson Laboratory	Cat# 022071; RRID: IMSR_JAX:022071
Oligonucleotides		
MiRCURY LNA *miR-19b-3p* Inhibitor	Qiagen	N/A
MirVana *miR-19b-3p* Mimic	Thermo Fisher Scientific	N/A
MirVana *miR-467f* Mimic	Thermo Fisher Scientific	N/A
Mouse *Il9* TaqMan Primer	Thermo Fisher Scientific	Cat# Mm00434305_m1
Mouse *Traf6* TaqMan Primer	Thermo Fisher Scientific	Cat# Mm00493836_m1
Mouse *Dbp* TaqMan Primer	Thermo Fisher Scientific	Cat# Mm00497539_m1
Mouse *E2f8* TaqMan Primer	Thermo Fisher Scientific	Cat# Mm01204160_m1
Mouse *Nlrc3* TaqMan Primer	Thermo Fisher Scientific	Cat# Mm00615968_m1
Mouse *Numbl* TaqMan Primer	Thermo Fisher Scientific	Cat# Mm00477931_m1
Mouse *Acta2* TaqMan Primer	Thermo Fisher Scientific	Cat# Mm01546133_m1
Mouse *Col1a1* TaqMan Primer	Thermo Fisher Scientific	Cat# Mm00801666_m1
Mouse *Col1a2* TaqMan Primer	Thermo Fisher Scientific	Cat# Mm00483888_m1
Mouse *Mmp2* TaqMan Primer	Thermo Fisher Scientific	Cat# Mm00439498_m1
Mouse *Mmp9* TaqMan Primer	Thermo Fisher Scientific	Cat# Mm00442991_m1
Mouse *Fn1* TaqMan Primer	Thermo Fisher Scientific	Cat# Mm01256744_m1
Mouse *Vmac* TaqMan Primer	Thermo Fisher Scientific	Cat# Mm01232760_m1
Mouse *Hprt* TaqMan Primer	Thermo Fisher Scientific	Cat# Mm00446968_m1
miR-19b-3p TaqMan Primer	Thermo Fisher Scientific	Cat# mmu478264_mir
miR-467f TaqMan Primer	Thermo Fisher Scientific	Cat# 002886
U6 snRNA TaqMan Primer	Thermo Fisher Scientific	Cat# 001973
Caenorhabditis elegans *miR-39-3p* TaqMan Primer	Thermo Fisher Scientific	Cat# 478293_mir
Human *IL9* TaqMan Primer	Thermo Fisher Scientific	Cat# Hs00174125_m1
Human *E2F8* TaqMan Primer	Thermo Fisher Scientific	Cat# Hs00226635_m1
Human *GAPDH* TaqMan Primer	Thermo Fisher Scientific	Cat# Hs99999905_m1
Recombinant DNA		
pMSCV-IRES-GFP-*Smad3*	Park et al.[5]	N/A
pMSCV-IRES-GFP-*Smad3* Mutations	Park et al.[5]	N/A
pMSCV-IRES-GFP-*E2f8*	Part et al.[5]	N/A
Software and algorithms		
FlowJo v10.9 Software	FlowJo	https://www.flowjo.com/solutions/flowjo/ RRID: SCR_008520

REAGENT or RESOURCE	SOURCE	IDENTIFIER
GraphPad Prism v8 Software	GraphPad Software	https://www.graphpad.com/ RRID: SCR_002798
QuantStudio 3 Real-Time PCR Software	Thermo Fisher Scientific	https://www.thermofisher.com/order/catalog/product/A28567#/A28567 RRID: SCR_018712
nCounter Analysis System	NanoString Technologies	https://www.nanostring.com/products/ncounter-analysis-system/ncounter-systems-overview/ RRID: SCR_021712
Leica Application Suite X Software	Leica Biosystems	https://www.leica-microsystems.com/products/microscope-software/details/product/leica-las-x-ls/ RRID: SCR_013673
NDP. View 2 Software	Hamamatsu	https://www.hamamatsu.com/eu/en/product/life-science-and-medical-systems/digital-slide-scanner/U12388-01.html
Other		
BD LSRFortessa	BD Biosciences	N/A
MACS Multistand	Miltenyi Biotec	Cat# 130-042-303
MACS MS Columns	Miltenyi Biotec	Cat# 130-042-201
Amersham Imager 680	Cytiva	N/A
QuantStudio 3 Real-Time PCR System	Thermo Fisher Scientific	Cat# A28567
NanoZoomer S60 Slide scanner	Hamamatsu	Cat# C13210-04
SpectraMax Plus 384 Microplate Reader	Molecular Devices	N/A
Synergy Microplate Reader	Bio Tex	N/A
Leica TCS SP8 X	Leica Microsystems	N/A
Graphical Abstract Illustration	Biorender	N/A